NASA TN D-1409

TECHNICAL NOTE

D-1409

COMBUSTION INSTABILITY LIMITS DETERMINED BY A NONLINEAR THEORY AND A ONE-DIMENSIONAL MODEL

By Richard J. Priem and Donald C. Guentert

Lewis Research Center
Cleveland, Ohio

NATIONAL AERONAUTICS AND SPACE ADMINISTRATION
WASHINGTON

October 1962

NATIONAL AERONAUTICS AND SPACE ADMINISTRATION

TECHNICAL NOTE D-1409

COMBUSTION INSTABILITY LIMITS DETERMINED BY A NONLINEAR THEORY AND A ONE-DIMENSIONAL MODEL

By Richard J. Priem and Donald C. Guentert

SUMMARY

Regions of combustion instability in rockets were calculated from a nonlinear theory that considered the combustor to be an annular section with very small thickness and length. Two models were used to determine the local burning rate. One assumed that the burning rate was equal to the vaporization rate; the other assumed that the burning rate was equal to the chemical-reaction rate. The results show that a finite disturbance is required to produce instability. The instability regions were found to be a function of several design parameters and to be insensitive to the activation energy, specific-heat ratio, and order of reaction of the propellants. The vaporization-rate model was more sensitive to a pressure disturbance for design parameters corresponding to conditions encountered in large combustors. The chemical-reaction-rate model was more sensitive to a pressure disturbance for conditions corresponding to small research combustors. Wave shapes and characteristics were determined for various conditions.

INTRODUCTION

A technique or theory to predict the occurrence of high-frequency combustion instability has been the goal of many researchers. To achieve this goal various investigators have taken different approaches. The concept of a control loop with a pressure-dependent time lag was used (refs. 1 and 2) to simulate the combustion processes. This approach gives stability limits in terms of the time lag but suffers from the disadvantage that one cannot relate the time lag to physical processes or combustor design parameters. Many investigators (refs. 3 to 13) have shown how processes that occur during combustion vary with pressure or velocity. These variations can sustain a wave by adding energy in phase with the wave. (This phenomenon is known as the Rayleigh criteria.) This approach has not yielded stability limits, and the results usually cannot be related to the design parameters. Another approach (refs. 14 to 16) uses similarity parameters to design a combustor that is similar

to a stable combustor. In practice, however, there are too many parameters to scale all terms directly. It has also been impossible to determine the stability limits as functions of the similarity parameters.

This report describes a theoretical investigation to predict and understand instability limits. The theory used many of the concepts previously mentioned. Transport equations similar to those used in references 5 and 6 are used to define the motion of the gases during instability. The equations are nondimensionalized to produce similarity parameters as in references 14 and 15. Finally, the mechanistic approach is used to define a model for the driving mechanism. Results from numerical calculations using the equations are then described to show the stability limits and other pertinent information as a function of the variables in the theory.

The combustor geometry considered was that of an annulus with small length and thickness. Mass was added to and removed from the annulus by flow in the axial direction. Because of the simplicity of the model, the results must be considered only as a rough indication of what occurs in a true three-dimensional combustor. The purposes of the one-dimensional combustor were to determine whether a finite disturbance is required to excite the instability and to determine which model for the driving mechanism is most important in producing instability. It was also anticipated that the one-dimensional analysis would indicate the importance of several design parameters and physical constants and would indicate simplifying assumptions applicable in the analysis of a two- or three-dimensional system.

SYMBOLS

A_c cross-sectional area of combustor, sq in.

A_p amplitude of pressure disturbance, dimensionless

A_t nozzle-throat area of combustor, sq in.

A_v amplitude of velocity disturbance, dimensionless

$\mathscr{A}$ combustor contraction ratio, A_c/A_t, dimensionless

a speed of sound in gases, in./sec

C mole fraction concentration of unburned gases, dimensionless

C_{dr} concentration of liquid drops, drops/cu in.

c_p specific heat at constant pressure, Btu/(lb)($^{\circ}$F)

c_v specific heat at constant volume, Btu/(lb)(^oF)

c^* characteristic exhaust velocity, ft/sec

D molecular diffusion coefficient, sq in./sec

E activation energy function in Arrhenius equation, ^oR

$f(\gamma)$ function of gamma, $\sqrt{\left(\frac{2}{\gamma + 1}\right)^{\frac{\gamma+1}{\gamma-1}}}$

g acceleration due to gravity, 386.09 in./sec^2

J mechanical equivalent of heat, 9339.1 in.-lb/Btu

$\mathscr{J}$ viscous-dissipation parameter, $\mu_0 c^*/r_{an}\bar{P}_c g$, dimensionless

k preexponential constant in Arrhenius equation, (cu in./lb)$^{n-1}$/sec

$\mathfrak{L}$ burning-rate parameter, $r_{an}m/\mathscr{J}$, dimensionless

M molecular weight of gas, lb mass/lb mole

M_l molecular weight of liquid, lb mass/lb mole

m burning rate of propellant, fraction/in.

n concentration exponent of Arrhenius equation, dimensionless

P pressure, lb/sq in.

P_v vapor pressure of liquid, lb/sq in.

q rate of heat transferred by conduction, Btu/(sec)(sq in.)

R universal gas constant, 18,510 (in.)(lb force)/(^oR)(lb mole)

r radial distance, in.

S surface area, sq in.

Sc Schmidt number, $\mu_0/D\rho_0$, dimensionless

T gas temperature, ^oR

t time, sec

t_i dummy variable of integration

U_l internal energy of liquid, Btu/lb

v gas velocity, in./sec

Δv velocity difference between gases and drops in axial direction, in./sec

v_l liquid velocity, in./sec

$\dot{W}$ propellant flow rate, lb/sec

α correction factor for mass transfer, $(P/P_v)\ln[P/(P - P_v)]$, dimensionless

γ specific-heat ratio, c_p/c_v, dimensionless

∇ operator, $(\text{in.})^{-1}$

λ thermal conductivity of gases, Btu/(in.)(sec)($^\circ$F)

μ gas viscosity, lb/(in.)(sec)

ρ gas density, lb/cu in.

ρ_l liquid density, lb/cu in.

τ stress tensor, lb/(in.)(sec^2)

ω local instantaneous burning rate for various combustion models, lb/(sec)(cu in.)

Subscripts:

an annulus

c combustion chamber

dr liquid drops

max maximum

min minimum

0 steady state

Superscript:

' reduced parameter, defined in eq. (A25)

— average

THEORY

The combustor geometry used in this investigation was an annular section with a very small thickness Δr and length Δz as shown in figure 1. The propellants are assumed to be uniformly introduced at the injector boundary and to burn at some rate, which depends on the position within the combustor. This is accompanied by gas and liquid flow in the axial direction. As the propellants burn, random disturbances occur within the combustor. If the amplitude of a disturbance is large enough, it may develop into a wave traveling within the combustor. The object of this study was to determine analytically the minimum amplitude of a pressure or a velocity disturbance in the annulus that is needed to develop into such a wave. This was accomplished by solving the transport equations, which are derived in appendixes A to C. Cylindrical coordinates are used in which the z-direction corresponds to the axial direction in the combustor. The following equations are the result:

Continuity:

$$\frac{\partial \rho'}{\partial t'} + \rho'\left(\frac{\partial v_\theta'}{\partial \theta'} + \frac{\partial v_z'}{\partial z'}\right) + v_\theta' \frac{\partial \rho'}{\partial \theta'} + v_z' \frac{\partial \rho'}{\partial z'} = \mathfrak{F}\omega' f(\gamma) \tag{1}$$

Momentum (in θ-direction):

$$\rho' \frac{\partial v_\theta'}{\partial t'} + \rho' v_\theta' \frac{\partial v_\theta'}{\partial \theta'} + \frac{1}{\gamma} \frac{\partial P'}{\partial \theta'} + \mathfrak{F}\omega' v_\theta' f(\gamma) = \frac{4}{3} \mathscr{J} \frac{\partial^2 v_\theta'}{(\partial \theta')^2} f(\gamma) \tag{2}$$

Energy:

$$\begin{aligned} \rho'\left(\frac{\partial T'}{\partial t'} + v_\theta' \frac{\partial T'}{\partial \theta'} + v_z' \frac{\partial T'}{\partial z'}\right) + (\gamma - 1)P'\left(\frac{\partial v_\theta'}{\partial \theta'} + \frac{\partial v_z'}{\partial z'}\right) &= \mathscr{J} \frac{\partial^2 T'}{(\partial \theta')^2} f(\gamma) \\ &+ \mathfrak{F}\omega'\left\{(\gamma - T') + \frac{\gamma - 1}{2} \gamma\left[(\Delta v')^2 + v_\theta'^2\right]\right\} f(\gamma) \\ &+ \frac{4}{3} \gamma(\gamma - 1) \mathscr{J}\left[\left(\frac{\partial v_\theta'}{\partial \theta'}\right)^2 + \left(\frac{\partial v_z'}{\partial z'}\right)^2 - \frac{\partial v_\theta'}{\partial \theta'} \frac{\partial v_z'}{\partial z'}\right] f(\gamma) \end{aligned} \tag{3}$$

Ideal gas:

$$\frac{\partial P'}{\partial \theta'} = T' \frac{\partial \rho'}{\partial \theta'} + \rho' \frac{\partial T'}{\partial \theta'} \tag{4}$$

The derivatives in the axial direction were determined with the assumption that the total mass, the momentum, and the energy in the annulus were constant. Furthermore, it was assumed that these derivatives were independent of r and θ. These assumptions result in the following equations (derived in appendix A), which permit evaluation of the derivatives taken with respect to z:

Continuity:

$$\frac{\partial v_z'}{\partial z} \int_0^{2\pi} \rho' \, d\theta' + 2\pi v_z' \frac{\partial \rho'}{\partial z'} = \mathfrak{L} f(\gamma) \int_0^{2\pi} \omega' \, d\theta' \tag{5}$$

Momentum:

$$v_z' \frac{\partial v'}{\partial z'} \int_0^{2\pi} \rho' \, d\theta' + \frac{1}{\gamma} \left(\frac{\partial \rho'}{\partial z'} \int_0^{2\pi} T' \, d\theta' + \frac{\partial T'}{\partial z'} \int_0^{2\pi} \rho' \, d\theta' \right)$$

$$= - \mathfrak{L} \, \Delta v' f(\gamma) \int_0^{2\pi} \omega' \, d\theta' \tag{6}$$

Energy:

$$v_z' \frac{\partial T'}{\partial z'} \int_0^{2\pi} \rho' \, d\theta' + (\gamma - 1) \frac{\partial v_z'}{\partial z'} \int_0^{2\pi} P' \, d\theta' = \frac{8\pi\gamma}{3} (\gamma - 1) \mathfrak{L} f(\gamma) \left(\frac{\partial v_z'}{\partial z'} \right)^2$$

$$+ \mathfrak{L} f(\gamma) \int_0^{2\pi} \omega' \left[(\gamma - T') + \gamma \frac{\gamma - 1}{2} (\Delta v')^2 \right] d\theta' \tag{7}$$

Ideal gas:

$$2\pi \frac{\partial P'}{\partial z'} = \frac{\partial \rho'}{\partial z'} \int_0^{2\pi} T' \, d\theta' + \frac{\partial T'}{\partial z'} \int_0^{2\pi} \rho' \, d\theta' \tag{8}$$

In addition to the transport equations given previously, an expression for the instantaneous local burning rate is required. Two models were used to compute the instantaneous burning rate. In the first model it was assumed that the vaporization rate varied with the amplitude of the disturbance and that the resulting vapor was instantly burned. The burning rate (i.e., the rate of appearance of burned gas) was thus limited by the vaporization rate. The vaporization rate was assumed to be proportional to the Reynolds number of the liquid drop. This implies that the temperature of the drops remained constant and also that the number and size of the drops entering the annulus remained constant. The burning rate is then given by the equation

$$\omega' = (\rho')^{1/2}\left[1 + \left(\frac{v'_\theta}{\Delta v'}\right)^2\right]^{1/4} \tag{9}$$

which is derived in appendix C.

In the second model it was assumed that the vaporization rate remained constant and that a disturbance changed only the rate of conversion of unburned gas into burned gas. The burning rate is then given by

$$\omega' = \left(\frac{C}{C_0}\right)^n (\rho')^n \exp\left[\frac{E}{RT_0}\left(1 - \frac{1}{T'}\right)\right] \tag{10a}$$

where

$$\frac{C}{C_0} = 1 + \frac{\mathfrak{C}}{C_0} f(\gamma) \int_0^{t'} \left(1 - \frac{\omega'}{\rho'}\right) dt'_i \tag{10b}$$

Equation (10b) determines the quantity of unburned gas, which varies with time. The average steady-state mole fraction concentration of unburned gases C_0 is given by

$$C_0^n = \frac{\omega_0}{\rho_0^{nk}} \exp\left(\frac{E}{RT_0}\right) \tag{10c}$$

These equations are derived in appendix C.

Two different types of disturbances were imposed. The first consisted of an instantaneous adiabatic pressure change at time $t' = 0$ given by:

$$P' = 1 + A_p \sin \theta' \tag{11a}$$

$$T' = (1 + A_P \sin \theta')^{(\gamma-1)/\gamma} \tag{11b}$$

$$\rho' = (1 + A_P \sin \theta')^{1/\gamma} \tag{11c}$$

$$v'_\theta = 0 \tag{11d}$$

The second type of disturbance consisted of an instantaneously imposed velocity component in the θ-direction

$$v_\theta = A_v \sin \theta \tag{12}$$

at constant pressure, temperature, and density.

For times greater than $t' = 0$ the pressure, the temperature, and the velocity at each position in the annulus were calculated by means of equations (1) to (9) with equations (9) or (10) and (11) or (12) on an IBM 704 numerical computer. The annulus was divided into 20 equal-sized increments. Time increments for stepwise integration varied with the values of $\mathfrak{L}$, C_0, and A_P and the model for burning rate as shown in figure 2. Smaller increments with large values of $\mathfrak{L}$ and A_P and small values of C_0 were required with the kinetics model in order to follow the rapid change in C as calculated by equation (10b). The computer times required to determine the condition to $t' = 2\pi$ are also shown in figure 2. Computations were always made up to a minimum of $t' = \pi$. With large time increments calculations were made to $t' = 10\pi$.

RESULTS AND DISCUSSION

The results of the numerical calculations were pressure, particle velocity, density, temperature, burning rate, and concentration at each of the 20 positions in the annulus as functions of time. Typical plots of pressure and velocity as functions of time for the various positions are shown in figures 3 and 4. The pressure wave can be observed to travel around the annulus; that is, the peak pressure point, which occurs at the 72° position at $t' = 6\pi$ radians, returns to the same position at $t' = 8\pi$ radians. The peak pressure point occurs at the opposite side of the annulus (252° position) at about 7π radians or 1/2 cycle after it occurs at the 72° position. Similar characteristics are observed for the gas velocity. Nodes are also observed for each wave; the pressure antinodes (i.e., the positions of maximum pressure fluctuations) occur at the 72° and 252° positions, while the velocity antinodes (i.e., the positions of maximum velocity variations) are at the 0° and 90° positions. The interactions of waves with each other through the nonlinear aspects of the equations produce considerable noise and distortion in the waves.

Typical pressure-position curves at a particular time are shown in figure 5. Figure 5(a) shows the pressure profile 6 periods after the initial disturbance occurred in a combustion chamber in which the burning rate is vaporization limited. At this time the wave has developed into a steep-fronted wave with a peak pressure 1.43 times the average pressure. There are also several waves of lower amplitude superimposed on the curve. Close examination of the results shows that these low-amplitude waves are decreasing with time.

The pressure profile obtained with the chemical-reaction-rate model is shown in figure 5(b). The wave is sinusoidal in shape, similar to the initial disturbance. A sinusoidal wave shape is also a characteristic of the pressure profiles for combustors with low burning-rate parameters, regardless of the model used for the burning rate.

Local pressure-time histories at a particular position in the combustor are shown in figure 6 for the same conditions as in figure 5. For a large burning-rate parameter the amplitude increases rapidly, and the wave shape becomes steep fronted, but for a low burning-rate parameter the amplitude increases very slowly.

To determine whether the amplitude of the wave increased with time, the peak pressure minus the minimum pressure (anywhere in the combustor) divided by the average pressure within the annulus was plotted as a function of time (fig. 7). Figure 7(a) shows the histories obtained with the vaporization model with various burning rates. The amplitude of the initial pressure disturbance was 10 percent of the average chamber pressure. For a low value of the burning-rate parameter (e.g., 0.028) the wave slowly decays. After a time of 10 periods the amplitude is about 9 percent of the average chamber pressure. Increasing the burning-rate parameter produces an unstable condition wherein the amplitude of the initial wave (viz., 10 percent of the chamber pressure) increases to a value of approximately 50 percent of the chamber pressure. As the burning-rate parameter is further increased, the system becomes more unstable; the pressure amplitude rises to a peak value in 1/2 cycle and stabilizes at an amplitude equal to the chamber pressure. A further increase in the burning-rate parameter produces a very stable condition in which the initial 10 percent disturbance decays to 1 percent of the chamber pressure in 1/5 cycle. Similar characteristics are obtained when the pressure disturbance is replaced by an initial-velocity disturbance with an amplitude equivalent to a Mach number of 0.02. These results are shown in figure 7(b).

Pressure histories for various values of the burning parameter using the chemical-reaction-rate model for the burning rate are shown in figure 7(c). For these cases the initial disturbance was 20 percent of the average chamber pressure (twice the value used with the vaporization model for fig. 7(a)). For low values of the burning-rate parameter the system is unstable, and the amplitude of the wave slowly increases. For

large values of the burning-rate parameter the system becomes stable; that is, the amplitude decays with time, the decay rate being proportional to the burning-rate parameter.

From curves similar to those shown in figures 5 to 7 it was possible to determine the values of minimum disturbance that would increase with time for a fixed set of constants. These values were used to define the boundaries for stable combustion. With the vaporization-rate model it was also possible to calculate the equilibrium wave amplitude (i.e., the condition where the amplitude did not change with time). The stability boundaries (minimum disturbance that would increase with time) and equilibrium amplitude for the vaporization model are shown in figure 8(a) for various values of the velocity difference between liquid and gas. Decreasing the velocity difference decreases the minimum pressure disturbance required to drive the system into instability and increases the equilibrium amplitude of the wave. A velocity difference of 0.01 (approximately 50 ft/sec) corresponds to the level of turbulence measured in the rocket combustor in reference 17, and also corresponds to turbulence in pipe flow. The curve also shows that the minimum disturbance required to excite instability has its lowest value at a burning-rate parameter of 0.8. The equilibrium amplitude increases with the burning-rate parameter and reaches values greater than the average chamber pressure at high values of the burning-rate parameter. These high equilibrium amplitudes could produce an order-of-magnitude increase in the heat-transfer rate as calculated from reference 18. This might explain how instability can produce burnout.

Figure 8(b) compares the results obtained with an initial pressure disturbance with those obtained with an initial velocity disturbance. The minimum amplitudes of the velocity and pressure disturbances that will increase with time are plotted on scales having corresponding energy levels. At low burning-rate parameters the stability boundaries for a velocity disturbance coincide with those obtained with a pressure disturbance. For higher values of the burning-rate parameters the minimum velocity disturbance required to produce instability is less than that required with a pressure disturbance. The equilibrium amplitude was the same with a velocity or a pressure disturbance. With a nonsinusoidal disturbance the stability boundaries corresponded to a sinusoidal disturbance with the same peak value of the disturbance.

The effect of other parameters appearing in the equations presented in the theory were also examined. A change in the specific-heat ratio γ from 1.0 to 1.5 had no noticeable effect on the minimum disturbance or equilibrium amplitude. Similarly, a change in the gas velocity from a Mach number of 0.01 to 0.7 (corresponding to velocities of 50 to 3500 ft/sec) had no effect on the stability limits of the system as long as the velocity difference between gas and liquid was held constant. Above velocities of Mach 0.7, the system became more stable, inasmuch as the minimum disturbance increased and the equilibrium amplitude

decreased. Changes in the viscous-dissipation parameter from 3×10^{-11} to 2×10^{-5} showed no effect on the stability limits. This was expected because the shear stresses in the one-dimensional model are negligible; thus there was negligible damping produced by viscous forces. Analysis of two- or three-dimensional systems will be required to show the effect of the viscous-dissipation parameter on the stability limits.

The stability limits for the chemical-reaction-rate model are shown in figure 8(c) for two values of the concentration of unburned gases. The minimum disturbance required to produce instability increases very rapidly with an increasing burning-rate parameter. The minimum disturbance required to excite instability also increased with decreasing concentration of unburned gases. The plots in figure 8(c) are for a concentration of unburned mixed gases of 0.1 or less. The 0.1 value corresponds to that calculated from equation (10c) with the largest expected evaporation rate (i.e., 100 lb/(cu in.)(sec)) and a large activation energy (viz., 100,000 cal/mole) for liquid propellants. The value of 0.1 could be exceeded with a premixed gaseous system. The effect of the order of the reaction n on the stability limits was insignificant between $n = 1.5$ and 2.5. Similarly, variations in the activation-energy term E/RT_0 from 2 to 10 showed a negligible change in the stability limits. The equilibrium amplitude was not determined for the chemical-reaction-rate model, because the unstable region occurred at low burning-rate parameters; for these conditions the amplitude increases so slowly that excessive computer time would be required to calculate the equilibrium value.

The minimum disturbance required to excite instability for either of the two models is shown in figure 8(d). At low burning-rate parameters a smaller disturbance will excite instability with the chemical-reaction-rate model than with the vaporization-rate model. At larger values of the burning-rate parameter a smaller disturbance will excite instability with the vaporization-rate model than with the chemical-reaction-rate model.

SUMMARY OF RESULTS

Instability regions were calculated from a nonlinear theory for an annular combustor with a very small thickness and length. Two combustor models were used to calculate the local instantaneous burning rate; for one model the burning rate was equated to the vaporization rate, and for the other the burning rate was equated to the chemical-reaction rate. The results indicate the following:

1. A finite pressure or a particle-velocity disturbance is required for a system to develop a high-amplitude wave traveling within the combustor. For disturbances below the minimum value the wave decays.

2. The minimum disturbance needed to excite instability is a function of the burning-rate parameter, the velocity difference between liquid drops and gas for a vaporization-rate combustor, and the concentration of unburned propellants for a chemical-reaction-rate combustor.

3. Other parameters (e.g., specific-heat ratio, gas velocity, activation energy, and order of the reaction) have a negligible influence on the stability limits of the system. The effect of viscous damping was negligible because the geometry considered did not include a boundary layer or other wall effects.

4. At low burning-rate parameters (a small-diameter combustor with a low burning rate and a large contraction ratio) a smaller disturbance will excite instability with the chemical-reaction-rate model than with the vaporization-rate model. With high burning-rate parameters a smaller disturbance will excite instability with the vaporization-rate model than with the chemical-reaction-rate model.

5. For low burning-rate parameters the wave shape is sinusoidal and the amplitude increases very slowly. With large burning-rate parameters the wave shape is very steep with peak amplitudes equal to the chamber pressure.

6. For burning-rate parameters between 1 and 10 an initial pressure disturbance of 2 to 10 percent of the average chamber pressure was required to produce instability. Above burning-rate parameters of 10 to 100, depending on the velocity difference between liquid and gas, the system is stable. A 10 percent disturbance decays to 1 percent in a fraction of a cycle.

CONCLUDING REMARKS

The results of this study also provide a means for estimating the effects of propellant properties and changes in combustion scale on system stability. These findings disclose that:

The minimum disturbance required to excite instability is affected by changing the propellant only because different propellants produce a different value of the burning-rate parameter and the value of the velocity difference between gases and drops; that is, a change in propellant density could influence the stability of a combustion system by changing the injection velocity, and thereby changing the velocity difference between the liquid and the gas.

The results have also shown that, with large combustors a model which assumes that the local burning rate is equal to the vaporization rate requires much smaller disturbances to produce instability than a

model that assumes the burning rate is equal to the chemical-reaction rate. For small-scale research combustors, however, the chemical-reaction-rate model requires a lower disturbance to excite instability than the vaporization model. Therefore, the application of experimental results obtained from small-scale research combustors may not be directly applicable to large combustors.

Lewis Research Center
National Aeronautics and Space Administration
Cleveland, Ohio, July 18, 1962

APPENDIX A

TRANSPORT EQUATIONS WITH MASS ADDITION

The transport equations with mass addition in which there is a phase change and energy release are developed in this appendix. The approach is similar to that used in reference 19; the nomenclature is that used in reference 19. The equations are derived in Cartesian coordinates in which the z-direction corresponds to the axial direction in a combustor.

Equation of Continuity

The continuity equation is derived by use of the flow model shown in sketch (a). The ρ and v terms refer to the density and velocity

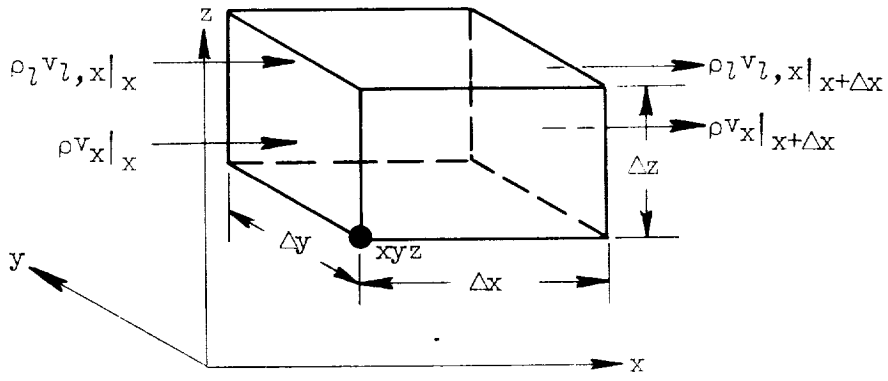

(a)

of the burned material, while ρ_l and v_l refer to the unburned material, liquid or gas.

This equation is developed by writing a mass-balance equation for a stationary volume element $\Delta x\, \Delta y\, \Delta z$ through which the fluid is moving as shown in sketch (a):

$$\begin{pmatrix}\text{Rate of mass}\\ \text{accumulation}\end{pmatrix} = \begin{pmatrix}\text{Rate of}\\ \text{mass in}\end{pmatrix} - \begin{pmatrix}\text{Rate of}\\ \text{mass out}\end{pmatrix} \qquad \text{(A1)}$$

For the pair of faces perpendicular to the x-axis the rate of mass in through the face is $\rho v_x|_x\, \Delta y\, \Delta z + \rho_l v_{l,x}|_x\, \Delta y\, \Delta z$, and the rate of mass out is $\rho v_x|_{x+\Delta x}\, \Delta y\, \Delta z + \rho_l v_{l,x}|_{x+\Delta x}\, \Delta y\, \Delta z$. Similar expressions can be

written for the other faces. Since the rate of mass accumulation is $\Delta x\ \Delta y\ \Delta z(\partial\rho/\partial t)$, the balance equation then becomes

$$\Delta x\ \Delta y\ \Delta z\ \frac{\partial \rho}{\partial t} = \Delta y\ \Delta z\left(\rho v_x\big|_x - \rho v_x\big|_{x+\Delta x} + \rho_l v_{l,x}\big|_x - \rho_l v_{l,x}\big|_{x+\Delta x}\right)$$

$$+ \Delta x\ \Delta y\left(\rho v_z\big|_z - \rho v_z\big|_{z+\Delta z} + \rho_l v_{l,z}\big|_z - \rho_l v_{l,z}\big|_{z+\Delta z}\right)$$

$$+ \Delta x\ \Delta z\left(\rho v_y\big|_y - \rho v_y\big|_{y+\Delta y} + \rho_l v_{l,y}\big|_y - \rho_l v_{l,y}\big|_{y+\Delta y}\right) \qquad \text{(A2)}$$

Dividing by $\Delta x\ \Delta y\ \Delta z$ and taking the limit as these dimensions approach zero results in

$$\frac{\partial \rho}{\partial t} = -\frac{\partial \rho v_x}{\partial x} - \frac{\partial \rho v_z}{\partial z} - \frac{\partial \rho v_y}{\partial y} - \frac{\partial \rho_l v_{l,x}}{\partial x} - \frac{\partial \rho_l v_{l,z}}{\partial z} - \frac{\partial \rho_l v_{l,y}}{\partial y} \qquad \text{(A3)}$$

The last three terms are the rate at which the unburned material disappears; this will be called the burning rate ω. Then the equation of continuity can be put in the following vector form:

$$\frac{\partial \rho}{\partial t} = -\nabla \cdot \rho\vec{v} + \omega \qquad \text{(A4)}$$

Equation of Motion

For a volume element $\Delta x\ \Delta y\ \Delta z$ the momentum-balance equation is

$$\begin{pmatrix}\text{Rate of}\\ \text{momentum}\\ \text{accumulation}\end{pmatrix} = \begin{pmatrix}\text{Rate of}\\ \text{momentum}\\ \text{in}\end{pmatrix} - \begin{pmatrix}\text{Rate of}\\ \text{momentum}\\ \text{out}\end{pmatrix} + \begin{pmatrix}\text{Sum of forces}\\ \text{acting on}\\ \text{system}\end{pmatrix} \qquad \text{(A5)}$$

and the flow model is

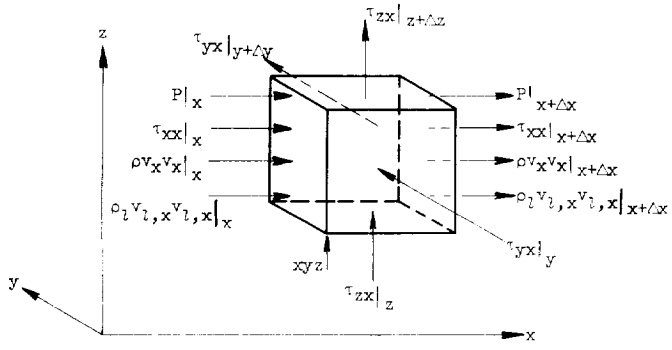

(b)

The flow of momentum in the x-direction is considered first. The rate at which momentum enters the yz-face at x is $(\rho v_x v_x + \rho_l v_{l,x} v_{l,x})\big|_x \Delta y\, \Delta z$, and the rate at which it leaves the yz-face at $x + \Delta x$ is $(\rho v_x v_x + \rho_l v_{l,x} v_{l,x})\big|_{x+\Delta x} \Delta y\, \Delta z$. Expressions for the other two faces are arrived at in a similar fashion. Hence, the net convective flow in the x-direction is

$$\Delta y\, \Delta z\left(\rho v_x v_x\big|_x - \rho v_x v_x\big|_{x+\Delta x} + \rho_l v_{l,x} v_{l,x}\big|_x - \rho_l v_{l,x} v_{l,x}\big|_{x+\Delta x}\right)$$

$$+ \Delta x\, \Delta z\left(\rho v_y v_x\big|_y - \rho v_y v_x\big|_{y+\Delta y} + \rho_l v_{l,y} v_{l,x}\big|_y - \rho_l v_{l,y} v_{l,x}\big|_{y+\Delta y}\right)$$

$$+ \Delta y\, \Delta x\left(\rho v_z v_x\big|_z - \rho v_z v_x\big|_{z+\Delta z} + \rho_l v_{l,z} v_{l,x}\big| - \rho_l v_{l,z} v_{l,x}\big|_{z+\Delta z}\right) \qquad (A6)$$

In order to obtain the net contribution of molecular transport to momentum in the x-direction, the rates at which momentum enters and leaves the various faces must be combined. The sum of these rates is

$$\Delta y\, \Delta z\left(\tau_{xx}\big|_x - \tau_{xx}\big|_{x+\Delta x}\right) + \Delta x\, \Delta z\left(\tau_{yx}\big|_y - \tau_{yx}\big|_{y+\Delta y}\right) + \Delta y\, \Delta x\left(\tau_{zx}\big|_z - \tau_{zx}\big|_{z+\Delta z}\right) \qquad (A7)$$

Fluid pressure is the only external force under consideration here; its effect on the yz-face is

$$g\, \Delta y\, \Delta z(P\big|_x - P\big|_{x+\Delta x}) \qquad (A8)$$

The rate of accumulation is

$$\Delta x\, \Delta y\, \Delta z\, \frac{\partial \rho v_x}{\partial t} \qquad (A9)$$

When the accumulation rate is equated to the sum of the other expressions (A6) to (A8) and the limit is taken as the volume size approaches zero,

$$\frac{\partial \rho v_x}{\partial t} = -\frac{\partial}{\partial x}\rho v_x v_x - \frac{\partial}{\partial y}\rho v_y v_x - \frac{\partial}{\partial z}\rho v_z v_x - \frac{\partial}{\partial x}\rho_l v_{l,x} v_{l,x} - \frac{\partial}{\partial y}\rho_l v_{l,y} v_{l,x}$$

$$- \frac{\partial}{\partial z}\rho_l v_{l,z} v_{l,x} - \frac{\partial}{\partial x}\tau_{xx} - \frac{\partial}{\partial y}\tau_{yx} - \frac{\partial}{\partial z}\tau_{zx} - g\frac{\partial P}{\partial x} \qquad (A10)$$

Comparable equations are obtained for the y- and z-directions; these are combined vectorially to give

$$\frac{\partial}{\partial t}\rho\vec{v} = -\nabla\cdot\rho\vec{v}\vec{v} - \nabla\cdot\rho_l\vec{v}_l\vec{v}_l - g\nabla P - \nabla\cdot\tau \qquad (A11)$$

Since

$$\nabla\cdot\rho_l\vec{v}_l\vec{v}_l = \vec{v}_l\nabla\cdot\rho_l\vec{v}_l + \rho_l\vec{v}_l\cdot\nabla\vec{v}_l \qquad (A12)$$

and the liquid velocity is assumed to be constant (i.e., $\vec{v}_l\cdot\nabla\vec{v}_l = 0$),

$$\nabla\cdot\rho_l\vec{v}_l\vec{v}_l = -\vec{v}_l\nabla\cdot\rho_l\vec{v}_l = -\vec{v}_l\omega \qquad (A13)$$

and

$$\frac{\partial\rho\vec{v}}{\partial t} = -\nabla\cdot\rho\vec{v}\vec{v} + \vec{v}_l\omega - g\nabla P - \nabla\cdot\tau \qquad (A14)$$

Expanding the first two terms of equation (A14) and using the continuity equation (Eq. (A4)) give

$$\rho\frac{\partial\vec{v}}{\partial t} = -\rho(\vec{v}\cdot\nabla)\vec{v} - (\vec{v}-\vec{v}_l)\omega - g\nabla P - \nabla\cdot\tau \qquad (A15)$$

Energy Equation

For a stationary volume element the law of conservation of energy states that

$$\begin{pmatrix}\text{Rate of accumulation of internal and kinetic energy}\end{pmatrix} = \begin{pmatrix}\text{Rate of internal and kinetic energy in by convection}\end{pmatrix} - \begin{pmatrix}\text{Rate of internal and kinetic energy out by convection}\end{pmatrix} + \begin{pmatrix}\text{Net rate of heat addition by conduction}\end{pmatrix} - \begin{pmatrix}\text{Net rate of work done by system on surroundings}\end{pmatrix}$$

The rate of accumulation of internal and kinetic energy is

$$\Delta x\,\Delta y\,\Delta z\,\frac{\partial}{\partial t}\left(\rho c_v T + \frac{1}{2gJ}\rho v^2\right) \qquad (A16)$$

The net rate of convection of internal and kinetic energy across the yz-faces is

$$\Delta y\ \Delta z\left[v_x\left(\rho c_v T + \frac{1}{2gJ}\ \rho v^2\right)\Big|_x - v_x\left(\rho c_v T + \frac{1}{2gJ}\ \rho v^2\right)\Big|_{x+\Delta x}\right]$$

$$+ \Delta y\ \Delta z\left[v_{l,x}\left(\rho_l U_l + \frac{1}{2gJ}\ \rho_l v_l^2\right)\Big|_x - v_{l,x}\left(\rho_l U_l + \frac{1}{2gJ}\ \rho_l v_l^2\right)\Big|_{x+\Delta x}\right] \tag{A17}$$

The net rate of energy input by conduction across the yz-faces is

$$\Delta y\ \Delta z\left(q_x|_x - q_x|_{x+\Delta x}\right) \tag{A18}$$

The rate of work done against static pressure is

$$\Delta y\ \Delta z\ \frac{1}{gJ}\left(Pv_x|_{x+\Delta x} - Pv_x|_x\right) \tag{A19}$$

Similarly the rate of work done against viscous forces is

$$\Delta y\ \Delta z\ \frac{1}{gJ}\left[(\tau_{xx}v_x + \tau_{xy}v_y + \tau_{xz}v_z)\Big|_{x+\Delta x} - (\tau_{xx}v_x + \tau_{xy}v_y + \tau_{xz}v_z)\Big|_x\right] \tag{A20}$$

Analogous expressions exist for the other two faces; adding these expressions for all faces and equating them to the expression for the rate of accumulation of internal and kinetic energy as the volume size approaches zero result in

$$\frac{\partial}{\partial t}\left(\rho c_v T + \frac{1}{2gJ}\ \rho v^2\right) = -\nabla \cdot \rho\vec{v}\left(c_v T + \frac{1}{2gJ}\ v^2\right)$$

$$- \nabla \cdot \rho_l \vec{v}_l\left(U_l + \frac{1}{2gJ}\ v_l^2\right) - \nabla \cdot \vec{q}$$

$$- \frac{1}{J}\nabla \cdot P\vec{v} - \frac{1}{gJ}\nabla \cdot (\tau \cdot v) \tag{A21}$$

Since

$$\nabla \cdot \rho_l \vec{v}_l \left(U_l + \frac{1}{2gJ} v_l^2\right) = \rho_l \vec{v}_l \cdot \nabla\left(U_l + \frac{1}{2gJ} v_l^2\right) + \left(U_l + \frac{1}{2gJ} v_l^2\right) \nabla \cdot \rho_l \vec{v}_l$$

and

$$\nabla \cdot \rho_l \vec{v}_l = -\omega$$

and for constant temperature and velocity of the unburned material

$$\nabla\left(U_l + \frac{1}{2gJ} v_l^2\right) = 0$$

then

$$\nabla \cdot \rho_l \vec{v}_l \left(U_l + \frac{1}{2gJ} v_l^2\right) = -\left(U_l + \frac{1}{2gJ} v_l^2\right)\omega \tag{A22}$$

and

$$\nabla \cdot \vec{q} = -\lambda \nabla^2 T \tag{A23}$$

When these equations are combined with the continuity and momentum equations,

$$\rho c_v \frac{\partial T}{\partial t} = -\rho c_v (\vec{v} \cdot \nabla) T + \lambda \nabla^2 T - \frac{P}{J} \nabla \cdot \vec{v}$$

$$- \frac{1}{gJ} \tau : \nabla \vec{v} + \omega\left[U_l - c_v T + \frac{1}{2gJ} (\vec{v}_l - \vec{v}) \cdot (\vec{v}_l - \vec{v})\right] \tag{A24}$$

Nondimensionalized Equations

The transport equations are nondimensionalized by means of the following transformations:

$$\left.\begin{aligned} t' &= ta/r_{an} & P' &= P/P_0 \\ \nabla' &= r_{an}\nabla & \tau' &= \tau r_{an}/\mu_0 a \\ \omega' &= \omega/\omega_0 & T' &= T/T_0 \\ \rho' &= \rho/\rho_0 & v' &= v/a \end{aligned}\right\} \tag{A25}$$

The resulting equations are:

Continuity:

$$\frac{\partial \rho'}{\partial t'} = -\nabla' \cdot \rho' \vec{v}' + \left| \frac{r_{an}\omega_0}{\rho_0 a} \right| \omega' \tag{A26}$$

Motion:

$$\rho' \frac{\partial \vec{v}'}{\partial t'} = -\rho'(\vec{v}' \cdot \nabla')\vec{v} - \left| \frac{g\overline{P}_c}{\rho_0 a} \right| \nabla' P' - \left| \frac{\mu}{r_{an}\rho_0 a} \right| \nabla' \cdot \tau' - \left| \frac{r_{an}\omega_0}{\rho_0 a} \right| (\vec{v}' - \vec{v}_l')\omega' \tag{A27}$$

Energy:

$$\rho' \frac{\partial T'}{\partial t'} = -\rho'(v' \cdot \nabla')T' + \left| \frac{\lambda}{r_{an}\rho_0 c_v a} \right| \nabla'^2 T - \left| \frac{\overline{P}_c}{\rho_0 c_v T_0 J} \right| P' \nabla' \cdot \vec{v}'$$

$$- \left| \frac{a\mu}{r_{an}\rho_0 c_v T_0 g J} \right| \tau' : \nabla' \vec{v}' + \left| \frac{\omega_0 r_{an}}{\rho_0 a} \right| \omega' \left[\frac{U_l}{c_v T_0} - T' + \left(\frac{a^2}{2gJc_v T_0} \right) (\vec{v}_l' - \vec{v}')^2 \right] \tag{A28}$$

In view of the fact that

$$gT_0 \frac{R}{M} \gamma = a^2 \qquad P = \rho \frac{R}{M} T$$

$$\frac{c_v \mu}{\lambda} \cong 1 \qquad U_l \cong c_p T_0$$

$$\frac{c_p}{c_v} = \gamma \qquad c_v = \frac{R}{JM}\left(\frac{1}{\gamma - 1} \right)$$

it follows that

$$\frac{g\overline{P}_c}{\rho_0 a^2} = \frac{1}{\gamma} \qquad \frac{\lambda}{r_{an}\rho_0 c_v a} = \frac{\mu}{r_{an}\rho_0 a}$$

$$\frac{\overline{P}_c}{\rho_0 c_v T_0 J} = \gamma - 1 \qquad \frac{a\mu}{r_{an}\rho_0 c_v T_0 g J} = \left(\frac{\mu}{r_{an}\rho_0 a} \right) \gamma(\gamma - 1)$$

For calculations based on the usual rocket combustor variables, it is convenient to transform the dimensionless groups above by applying the following expressions

$$c^* = \frac{\bar{P}_c A_t g}{\dot{W}} = \frac{1}{\gamma}\sqrt{\frac{g\gamma R T_0}{M\left(\frac{\gamma}{\gamma+1}\right)^{\frac{\gamma+1}{\gamma-1}}}}$$

$$\omega_0 = m\frac{\dot{W}}{A_c}$$

$$P_0 = \rho_0 \frac{R}{M} T_0$$

$$\mathscr{A} = \frac{A_c}{A_t}$$

$$a^2 = g\frac{R}{M}\gamma T_0$$

which results in

$$\frac{r_{an}\omega_0}{\rho_0 a} = \frac{r_{an}^m}{\mathscr{A}}\sqrt{\left(\frac{2}{\gamma+1}\right)^{\frac{\gamma+1}{\gamma-1}}} = \frac{r_{an}^m}{\mathscr{A}} f(\gamma) \qquad \text{(A29)}$$

and

$$\frac{\mu}{\rho_0 r_{an}^a} = \frac{\mu c^*}{r_{an}\bar{P}_c g}\sqrt{\left(\frac{2}{\gamma+1}\right)^{\frac{\gamma+1}{\gamma-1}}} = \frac{\mu c^*}{r_{an}\bar{P}_c g} f(\gamma) \qquad \text{(A30)}$$

For a given propellant combination only the following terms change with combustor design:

$$\frac{r_{an}^m}{\mathscr{A}} \equiv \mathfrak{L} \qquad \text{(A31)}$$

and

$$\frac{\mu c^*}{r_{an}\overline{P}_c g} \equiv \mathcal{J} \tag{A32}$$

The first term $\mathcal{L}$ is a burning-rate parameter, and $\mathcal{J}$ is a viscous-dissipation parameter. They are similar to Damköhlers' third group and Reynolds number except that they are based on the speed of sound rather than the gas velocity. The burning-rate parameter $\mathcal{L}$ is a measure of the energy that can be added to a wave by combustion, while the viscous-dissipation parameter $\mathcal{J}$ is a measure of the energy lost by viscous forces. The transport equations then become

Continuity:

$$\frac{\partial \rho'}{\partial t'} = -\nabla' \cdot \rho' \vec{v}' + \omega' \mathcal{L} f(\gamma) \tag{A33}$$

Motion:

$$\rho' \frac{\partial \vec{v}'}{\partial t'} = -\rho'(\vec{v}' \cdot \nabla')\vec{v}' - \frac{1}{\gamma} \nabla' P' - \mathcal{J} f(\gamma) \nabla' \cdot \tau' - (\vec{v}' - \vec{v}_l')\omega' \mathcal{L} f(\gamma) \tag{A34}$$

Energy:

$$\rho' \frac{\partial T'}{\partial t'} = -\rho'(\vec{v}' \cdot \nabla')T' + \nabla'^2 T \mathcal{J} f(\gamma) - |\gamma - 1| P' \nabla' \cdot \vec{v}'$$

$$- |\gamma(\gamma - 1)| \mathcal{J} f(\gamma) \tau' : (\nabla' \vec{v}') + \mathcal{L} f(\gamma) \omega' \left[\gamma - T' + \frac{(\gamma - 1)\gamma}{2} (v_l' - \vec{v}')^2 \right] \tag{A35}$$

APPENDIX B

TRANSPORT EQUATIONS FOR ANNULAR MODEL

For the annular combustor considered herein, the radial velocity v_r and all derivatives in the radial direction $\partial/\partial r$ are assumed to be zero. It is also assumed that the axial velocity does not vary with angular position $\partial v_z/\partial\theta = 0$ and that all second derivatives in the axial direction are zero. For the annular combustor where $r_c = r_{an}$ and the reduced radial distance r' is always unity, these transport equations are

Continuity:

$$\frac{\partial\rho'}{\partial t'} = -\rho'\left(\frac{\partial v'_\theta}{\partial\theta'} + \frac{\partial v'_z}{\partial z'}\right) - v'_\theta \frac{\partial\rho'}{\partial\theta'} - v'_z \frac{\partial\rho'}{\partial z'} + \omega' \mathfrak{L} f(\gamma) \tag{B1}$$

Momentum (in the θ-direction):

$$\rho' \frac{\partial v'_\theta}{\partial t'} = -\rho v'_\theta \frac{\partial v'_\theta}{\partial\theta'} - \left|\frac{1}{\gamma}\right| \frac{\partial P'}{\partial\theta'} + \mathscr{J} f(\gamma) \frac{4}{3} \frac{\partial^2 v'_\theta}{(\partial\theta')^2} - v'_\theta \omega' \mathfrak{L} f(\gamma) \tag{B2}$$

Momentum (in the axial or z-direction):

$$0 = -\rho' v'_z \frac{\partial v'_z}{\partial z'} - \left|\frac{1}{\gamma}\right| \frac{\partial P'}{\partial z'} - \mathfrak{L} f(\gamma)(v'_z - v'_l)\omega' \tag{B3}$$

Energy:

$$\rho' \frac{\partial T'}{\partial t'} = -\rho'\left(v'_\theta \frac{\partial T'}{\partial\theta'} + v'_z \frac{\partial T'}{\partial z'}\right) + \mathscr{J} f(\gamma) \frac{\partial^2 T'}{(\partial\theta')^2} - |\gamma - 1| P'\left(\frac{\partial v'_\theta}{\partial\theta'} + \frac{\partial v'_z}{\partial z'}\right)$$

$$+ \frac{4}{3}|\gamma(\gamma - 1)| \mathscr{J}\left[\left(\frac{\partial v'_\theta}{\partial\theta'}\right)^2 + \left(\frac{\partial v'_z}{\partial z'}\right)^2 - \frac{\partial v'_\theta}{\partial\theta'} \frac{\partial v'_z}{\partial z'}\right] f(\gamma)$$

$$+ \mathfrak{L} f(\gamma)\omega'\left\{\gamma - T' + \frac{(\gamma - 1)\gamma}{2}\left[(v'_l - v'_z)^2 + v'^2_\theta\right]\right\} \tag{B4}$$

Conservation of energy, momentum, and mass must apply for the entire system as well as the incremental volumes. Therefore, to determine the derivatives in the axial or z-direction, the conservation equations are integrated through the entire volume of the annulus. Since it is assumed

that none of the terms vary in the axial or radial direction, the equations only have to be integrated in the θ-direction. The equations become:

Continuity:

$$\int_0^{2\pi} \frac{\partial \rho'}{\partial t'}\, d\theta' = \int_0^{2\pi} \left[-\rho'\left(\frac{\partial v'_\theta}{\partial \theta'} + \frac{\partial v'_z}{\partial z'}\right) - v'_\theta \frac{\partial \rho'}{\partial \theta'} - v'_z \frac{\partial \rho'}{\partial z'} + \omega' \mathcal{L} f(\gamma)\right] d\theta' \tag{B5}$$

Momentum (in the z-direction):

$$0 = -\int_0^{2\pi} \left[\rho' v'_z \frac{\partial v'_z}{\partial z'} + \frac{1}{\gamma}\frac{\partial P'}{\partial z'} + \mathcal{L} f(\gamma)(v'_z - v'_l)\omega'\right] d\theta' \tag{B6}$$

Energy:

$$\int_0^{2\pi} \rho' \frac{\partial T'}{\partial t'}\, d\theta' = \int_0^{2\pi} \left(-\rho'\left(v'_\theta \frac{\partial T'}{\partial \theta'} + v'_z \frac{\partial T'}{\partial z'}\right) + \frac{\partial^2 T'}{(\partial \theta')^2} \mathcal{J} f(\gamma)\right.$$

$$- (\gamma - 1)P'\left(\frac{\partial v'_\theta}{\partial \theta'} + \frac{\partial v'_z}{\partial z'}\right) + \frac{4}{3}\gamma(\gamma - 1) f(\gamma) \mathcal{J}\left[\left(\frac{\partial v'_\theta}{\partial \theta'}\right)^2 + \left(\frac{\partial v'_z}{\partial z'}\right) - \frac{\partial v'_\theta}{\partial \theta'}\frac{\partial v'_z}{\partial z'}\right]$$

$$\left. + \omega' \mathcal{L} f(\gamma)\left\{\gamma - T' + \frac{(\gamma - 1)\gamma}{2}\left[(v'_l - v'_z) + v'_\theta\right]\right\}\right) d\theta' \tag{B7}$$

Ideal gas:

$$\int_0^{2\pi} \frac{\partial P'}{\partial z'}\, d\theta' = \int_0^{2\pi} \left(\frac{\partial P'}{\partial z'} T' + \frac{\partial T'}{\partial z'} \rho'\right) d\theta' \tag{B8}$$

Now it is assumed that the total mass, momentum, and energy in the annulus does not vary with time so that all the terms in the left side of equations (B5) to (B7) are zero. It is also assumed that none of the terms vary in the small distances $\Delta r_c'$ and $\Delta z'$ and that $\partial T'/\partial z'$, $\partial v_z'/\partial z'$, $\partial \rho'/\partial z'$, and $\partial P'/\partial z'$ do not vary with angular position (they are average values). Furthermore, there can be no net loss or gain of energy, mass, or momentum fluxes in the angular (θ) direction since the system is closed in that direction. This results in the equations

Continuity:

$$0 = -\frac{\partial v_z'}{\partial z'} \int_0^{2\pi} \rho' \, d\theta' - 2\pi v_z' \frac{\partial \rho'}{\partial z'} + \mathfrak{L} f(\gamma) \int_0^{2\pi} \omega' \, d\theta' \tag{B9}$$

Momentum:

$$0 = -\frac{\partial v_z'}{\partial z'} v_z' \int_0^{2\pi} \rho' \, d\theta' - \frac{1}{\gamma}\left(\frac{\partial \rho'}{\partial z'} \int_0^{2\pi} T' \, d\theta' + \frac{\partial T'}{\partial z'} \int_0^{2\pi} \rho' \, d\theta'\right)$$

$$- \mathfrak{L} f(\gamma)(v_z' - v_l') \int_0^{2\pi} \omega' \, d\theta' \tag{B10}$$

Energy:

$$0 = -\frac{\partial T'}{\partial z'} v_z' \int_0^{2\pi} \rho' \, d\theta' - (\gamma - 1) \frac{\partial v_z'}{\partial z'} \int_0^{2\pi} P' \, d\theta'$$

$$+ \frac{8\pi}{3} |\gamma(\gamma - 1)| \mathfrak{L} f(\gamma) \left(\frac{\partial v_z'}{\partial z'}\right)^2$$

$$+ \mathfrak{L} f(\gamma) \int_0^{2\pi} \omega' \left[\gamma - T' + (\gamma - 1) \frac{\gamma}{2} (v_l - v_z)^2\right] d\theta' \tag{B11}$$

Ideal gas:

$$2\pi \frac{\partial P'}{\partial z'} = \frac{\partial \rho'}{\partial z'} \int_0^{2\pi} T' \, d\theta' + \frac{\partial T'}{\partial z'} \int_0^{2\pi} \rho' \, d\theta' \tag{B12}$$

APPENDIX C

EQUATIONS FOR MASS ADDITION

Vaporization Model

The rate of propellant vaporization can be determined by the following equation from reference 20:

$$\omega = \frac{C_{dr} D M_l \bar{S}_{dr}^{\alpha}}{RT 2 r_{dr}} P_v \left[2 + 0.6\, Sc^{1/3} \left(\frac{2 r_{dr} |\vec{v} - \vec{v}_l| \rho}{\mu} \right)^{1/2} \right] \tag{C1}$$

If the liquid temperature and vapor pressure do not vary with time, the following nondimensional vaporization rate is obtained:

$$\omega' = \frac{\omega}{\omega_0} = \frac{2 + 0.6\, Sc^{1/3} \left(2 r_{dr} |\vec{v} - \vec{v}_l| \frac{\rho}{\mu} \right)^{1/2}}{2 + 0.6\, Sc^{1/3} \left(2 r_{dr} |\vec{v}_0 - \vec{v}_{l,0}| \frac{\rho}{\mu} \right)^{1/2}} \tag{C2}$$

For large velocity differences or Reynolds numbers the 2 in equations (C1) and (C2) can be neglected; then

$$\omega' = \left(\frac{\rho}{\rho_0} \right)^{1/2} \left(\frac{|\vec{v} - \vec{v}_l|}{|\vec{v}_0 - \vec{v}_l|} \right)^{1/2} \tag{C3}$$

In this analysis the liquid velocity is assumed to be axial (z-direction only) and constant. For the undisturbed case the transverse gas velocity is zero and

$$\omega' = (\rho')^{1/2}\left(\frac{|\vec{v}_\theta + \vec{v}_z - \vec{v}_l|}{|\vec{v}_z - \vec{v}_l|}\right)^{1/2}$$

$$= (\rho')^{1/2}\left(\frac{|\vec{v}_\theta + \Delta\vec{v}|}{|\Delta\vec{v}|}\right)^{1/2}$$

$$= (\rho')^{1/2}\left[\left(\frac{v_\theta^2 + \Delta v^2}{\Delta v^2}\right)^{1/2}\right]^{1/2}$$

$$= (\rho')^{1/2}\left(\frac{v_\theta^2 + \Delta v^2}{\Delta v^2}\right)^{1/4}$$

$$= (\rho')^{1/2}\left[1 + \left(\frac{v_\theta}{\Delta v}\right)^2\right]^{1/4} \tag{C4}$$

$$\omega' = (\rho')^{1/2}\left[1 + \left(\frac{v'_\theta}{\Delta v'}\right)^2\right]^{1/4} \tag{9}$$

Chemical Kinetics

The chemical-reaction rate is given by the Arrhenius equation

$$\omega = kC^n\rho^n \exp\left(-\frac{E}{RT}\right) \tag{C5}$$

and the average rate is

$$\omega_0 = kC_0^n\rho_0^n \exp\left(-\frac{E}{RT_0}\right) \tag{C6}$$

then

$$\omega' = \frac{\omega}{\omega_0} = \left(\frac{C}{C_0}\right)^n(\rho')^n \exp\left[\frac{E}{RT_0}\left(1 - \frac{1}{T'}\right)\right] \tag{10a}$$

If the flow of unburned gas into a unit volume is constant and equal to ω_0, the concentration within a unit volume at any time is

$$C = C_0 + \int_0^t \left(\frac{\omega_0}{\rho_0} - \frac{\omega}{\rho}\right) dt_i \tag{C7}$$

$$\frac{C}{C_0} = 1 + \frac{\omega_0}{\rho_0 C_0} \int_0^t \left(1 - \frac{\omega'}{\rho'}\right) dt_i \tag{C8}$$

In nondimensional form

$$\frac{C}{C_0} = 1 + \mathfrak{L} f(\gamma) \frac{1}{C_0} \int_0^{t'} \left(1 - \frac{\omega'}{\rho'}\right) dt_i' \tag{C9}$$

where C_0 is determined by

$$C_0^n = \frac{\omega_0}{\rho_0^{n_k}} \exp\left(\frac{E}{RT_0}\right) \tag{10c}$$

REFERENCES

1. Crocco, Luigi, Cheng, Sin-I.: Theory of Combustion Instability in Liquid Propellant Rocket Motors. Agardograph 8, Butterworth Sci. Pub. (London), 1956.

2. Summerfield, Martin: A Theory of Unstable Combustion in Liquid Propellant Rocket Systems. Jour. Am. Rocket Soc., vol. 21, no. 5, Sept. 1951, pp. 108-114.

3. Krieg, H. C., Jr.: The Tangential Mode of Combustion Instability. Paper 1723-61, Am. Rocket Soc., Inc., 1961.

4. Pickford, R. S., and Peoples, R. G.: Inherent Stability of the Combustion Process. Paper 1490-60, Am. Rocket Soc., Inc., 1960.

5. Rabin, E., Schallenmuller, A. R., and Lawhead, R. B.: Displacement and Shattering of Propellant Droplets. TR 60-75, Office Sci. Res., Mar. 1960.

6. Kumagai, Seiichiro, and Isoda, Hiroshi: Combustion of Fuel Droplets in a Vibrating Air Field. Fifth Symposium (International) on Combustion, Reinhold Publ. Corp., 1955, pp. 129-132.

7. Agoston, G. A., Wise, H. K., and Rosser, W. A.: Dynamic Factors Affecting the Combustion of Liquid Spheres. Sixth Symposium (International) on Combustion, Reinhold Publ., Corp., 1957, pp. 708-716.

8. Wharton, Walter W., Connaughton, J. W., Allan, B. D., and Williams, W. D.: The Effect of Sound Oscillations on Combustion and Heat Transfer. TR 1C36R, Army Rocket and Guided Missile Agency, Dec. 15, 1959.

9. Osborn, J. R., and Pinchak, A. C.: Investigation of Aerothermodynamics Interaction Phenomena in Combustion Pressure Oscillations. Rep. 1-59-2, Purdue Univ., June 1959.

10. Imber, M.: Combustion Instability: Liquid Stream and Droplet Behavior. Pt. II. Estimating Primary Liquid Jet Break Up with Heat Transfer Considerations. TR 59-720, WADC, Sept. 1960.

11. Reba, Imants, and Brosilow, Coleman: Combustion Instability: Liquid Stream and Droplet Behavior. Pt. III. The Response of Liquid Jets to Large Amplitude Sonic Oscillations. TR 59-720, WADC, Sept. 1960.

12. Wieber, Paul R., and Mickelsen, William R.: Effect of Transverse Acoustic Oscillations on the Vaporization of a Liquid-Fuel Droplet. NASA TN D-287, 1960.

13. Morrell, G.: Breakup of Liquid Jets by Transverse Shocks. Eighth Symposium (International) on Combustion, The Williams & Wilkins Co., 1962, pp. 1059-1067.

14. Ross, Chandler C., and Datner, Paul P.: Combustion Instability in Liquid-Propellant Rocket Motors - A Survey. Selected Combustion Problems - Fundamentals and Aero. Applications. Butterworths Sci. Pub., 1954, pp. 352-380; discussion, pp. 381-402.

15. Penner, S. S.: Rational Scaling Procedures for Liquid-Fuel Rocket Engines. Jet Prop., vol. 27, no. 2, pt. I, Feb. 1957, pp. 156-161.

16. Priem, Richard J., and Morrell, Gerald: Application of Similarity Parameters for Correlating High-Frequency Instability Behavior of Liquid Propellant Combustors. Paper 1721-61, Am. Rocket Soc., Inc., 1961.

17. Hersch, Martin: An Experimental Method of Measuring Intensity of Turbulence in a Rocket Chamber. ARS Jour., vol. 31, no. 1, Jan. 1961, pp. 39-46.

18. Feiler, Charles E., and Yeager, Ernest B.: Effect of Large-Amplitude Oscillations on Heat Transfer. NASA TR R-142, 1962.

19. Bird, R. B., Stewart, W. E., and Lightfoot, E. N.: Transport Phenomena. John Wiley & Sons, Inc., 1960.

20. Priem, Richard J., and Heidmann, Marcus F.: Propellant Vaporization as a Design Criterion for Rocket-Engine Combustion Chambers. NASA TR R-67, 1960. (Supersedes NACA TN's 3883, 3985, 4098, and 4219.)

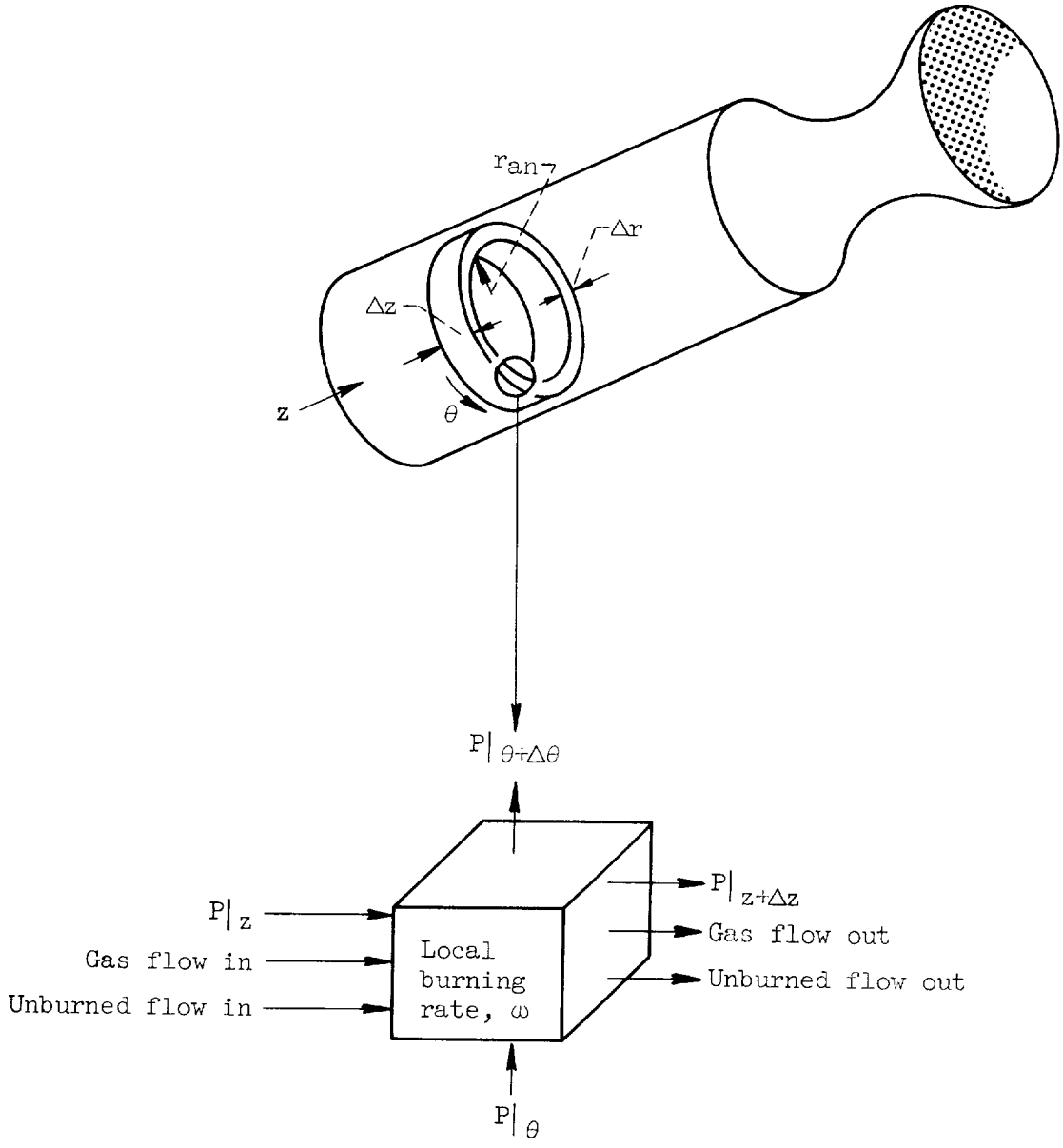

Figure 1. - Schematic diagram of model for instability.

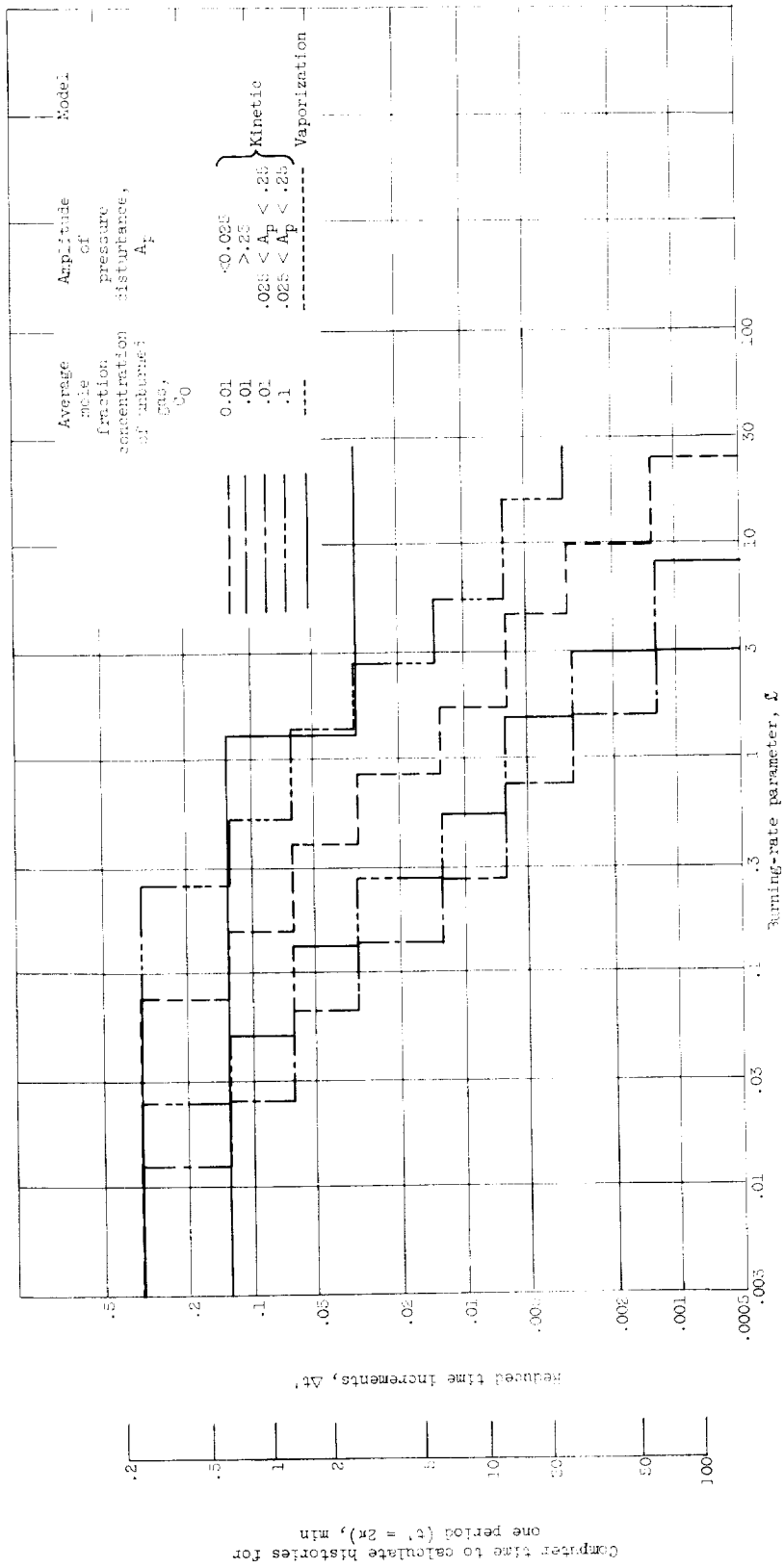

Figure 2. - Step sizes used in calculations.

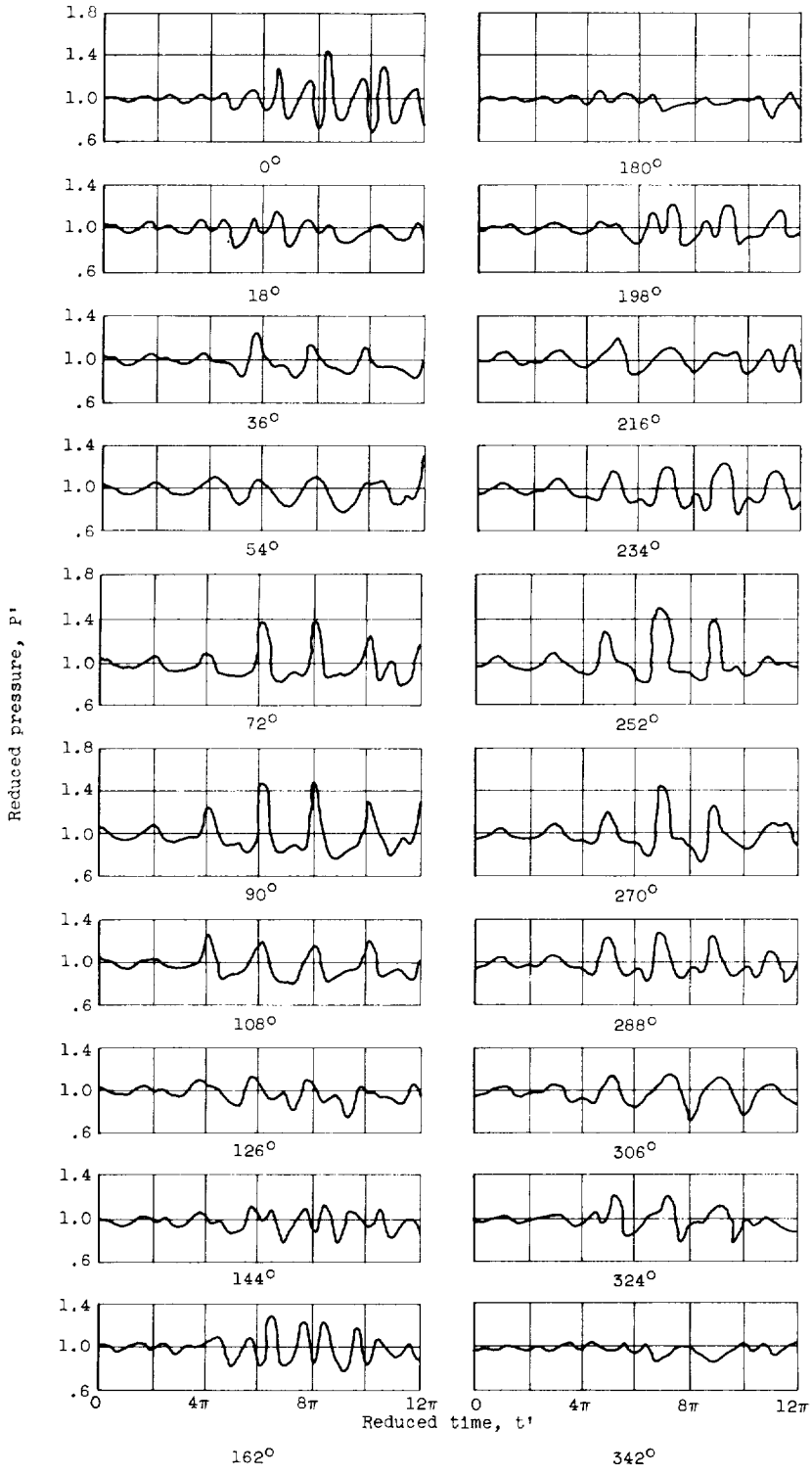

Figure 3. - Reduced pressure as function of reduced time at various positions. Burning-rate parameter, 0.28; viscous-dissipation parameter, 0.3×10^{-7}; reduced average gas velocity, 0.05; reduced velocity difference between gases and drops in axial direction, 0.02; specific-heat ratio, 1.2; vaporization-rate model.

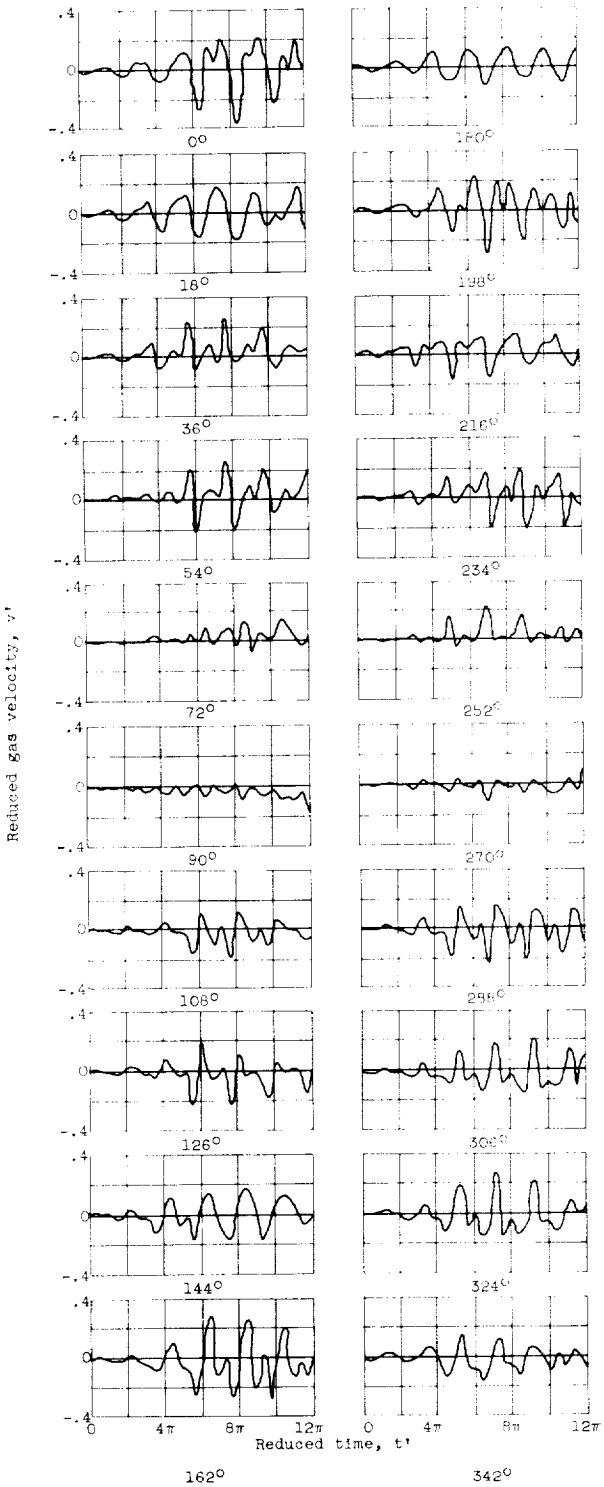

Figure 4. - Reduced gas velocity as function of reduced time at various positions. Burning-rate parameter, 0.28; viscous-dissipation parameter, 0.3×10^{-7}; reduced average gas velocity, 0.08; reduced velocity difference between gases and drops in axial direction, 0.02; specific-heat ratio, 1.2; vaporization-rate model.

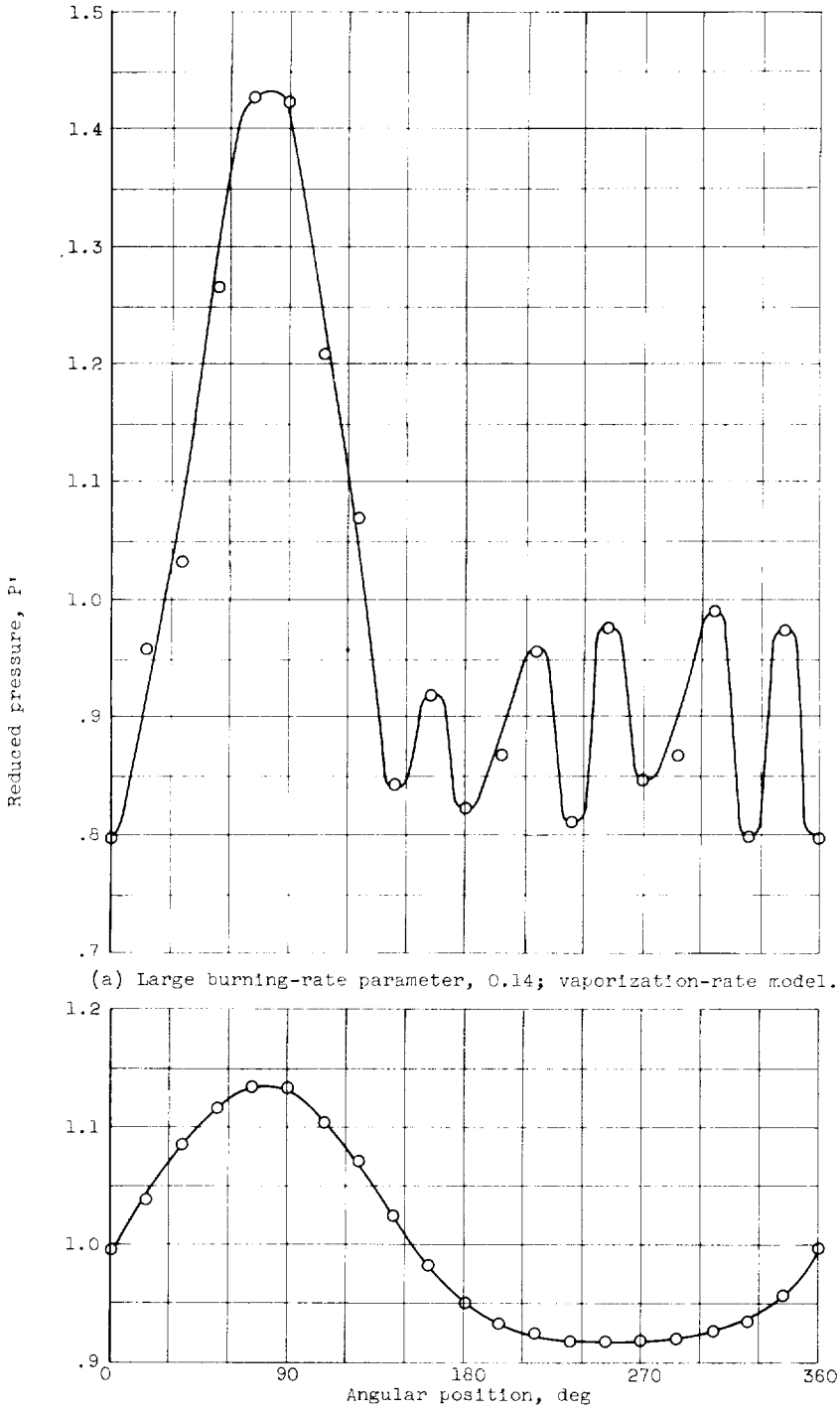

(a) Large burning-rate parameter, 0.14; vaporization-rate model.

(b) Small burning-rate parameter, 0.028; chemical-reaction-rate model. Average mole fraction concentration of unburned gases, 0.1.

Figure 5. - Typical pressure-position curves. Viscous-dissipation parameter, 0.3×10^{-7}; reduced average gas velocity, 0.05; reduced velocity difference between gases and drops in axial direction, 0.02; specific-heat ratio, 1.2; time, 6 periods or 12π.

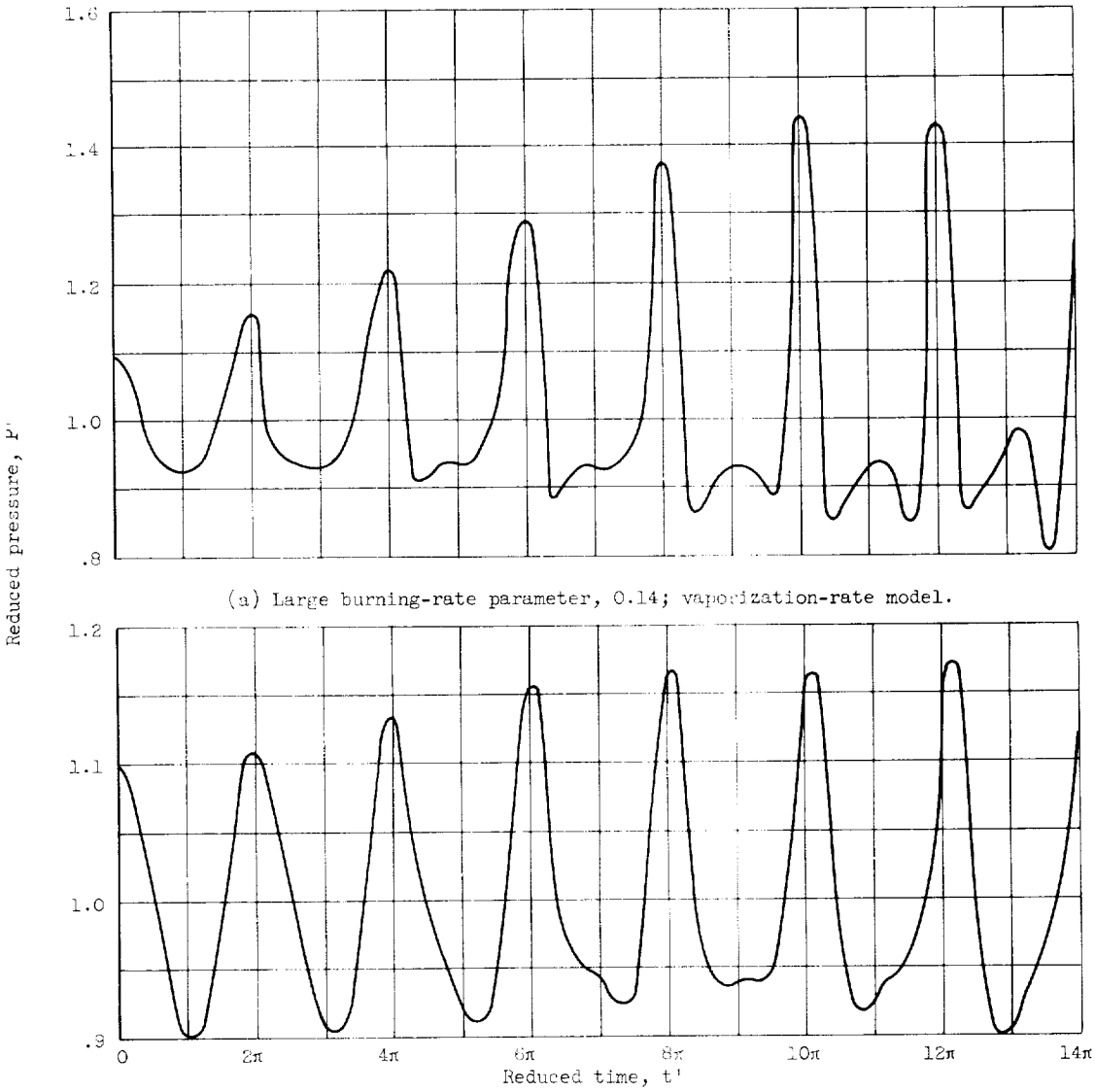

(a) Large burning-rate parameter, 0.14; vaporization-rate model.

(b) Small burning-rate parameter, 0.028; chemical-reaction-rate model. Average mole fraction concentration of unburned gases, 0.1.

Figure 6. - Typical local pressure-time histories. Viscous-dissipation parameter, 0.3×10^{-7}; reduced average gas velocity, 0.05; reduced velocity difference between gases and drops in axial direction, 0.02; specific-heat ratio, 1.2; position, 72°.

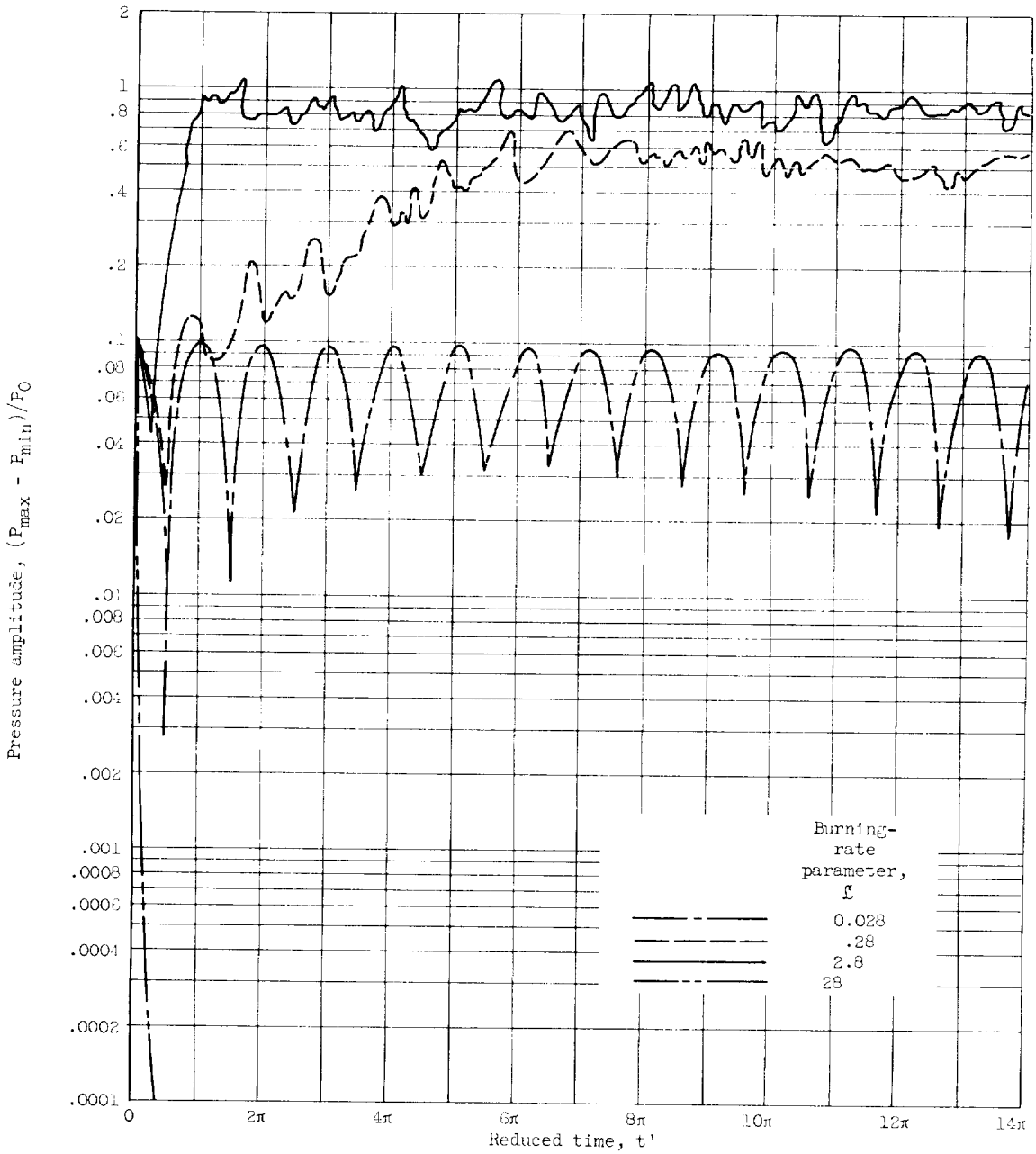

(a) Vaporization-rate model; initial pressure disturbance.

Figure 7. - Pressure-amplitude - time histories. Viscous-dissipation parameter, 0.3×10^{-7}; reduced average gas velocity, 0.05; reduced velocity difference between gases and drops in axial direction, 0.02; specific-heat ratio, 1.2.

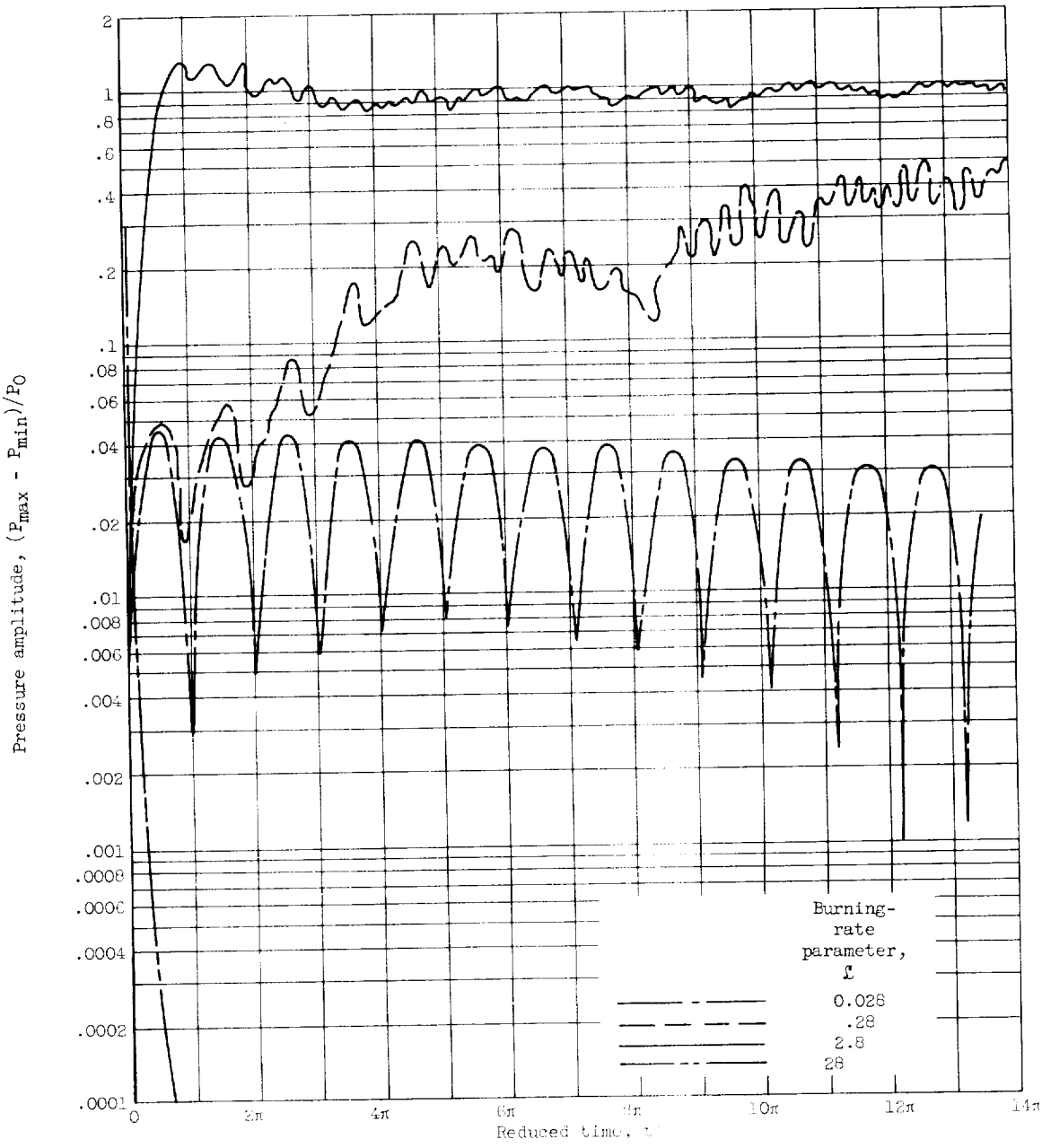

(b) Vaporization-rate model; initial particle-velocity disturbance.

Figure 7. - Continued. Pressure-amplitude - time histories. Viscous-dissipation parameter, 0.3×10^{-7}; reduced average gas velocity, 0.05; reduced velocity difference between gases and drops in axial direction, 0.02; specific-heat ratio, 1.2.

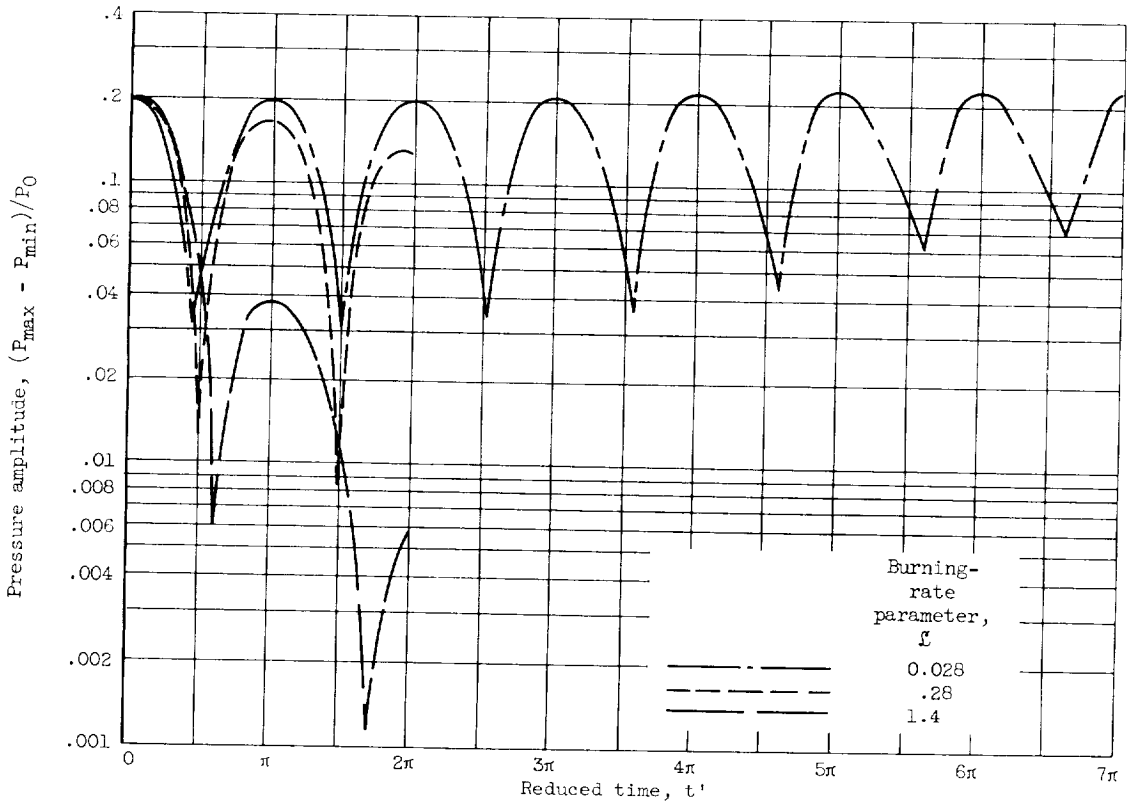

(c) Chemical-reaction-rate model; initial pressure disturbance.

Figure 7. - Concluded. Pressure-amplitude - time histories. Viscous-dissipation parameter, 0.3×10^{-7}; reduced average gas velocity, 0.05; reduced velocity difference between gases and drops in axial direction, 0.02; specific-heat ratio, 1.2.

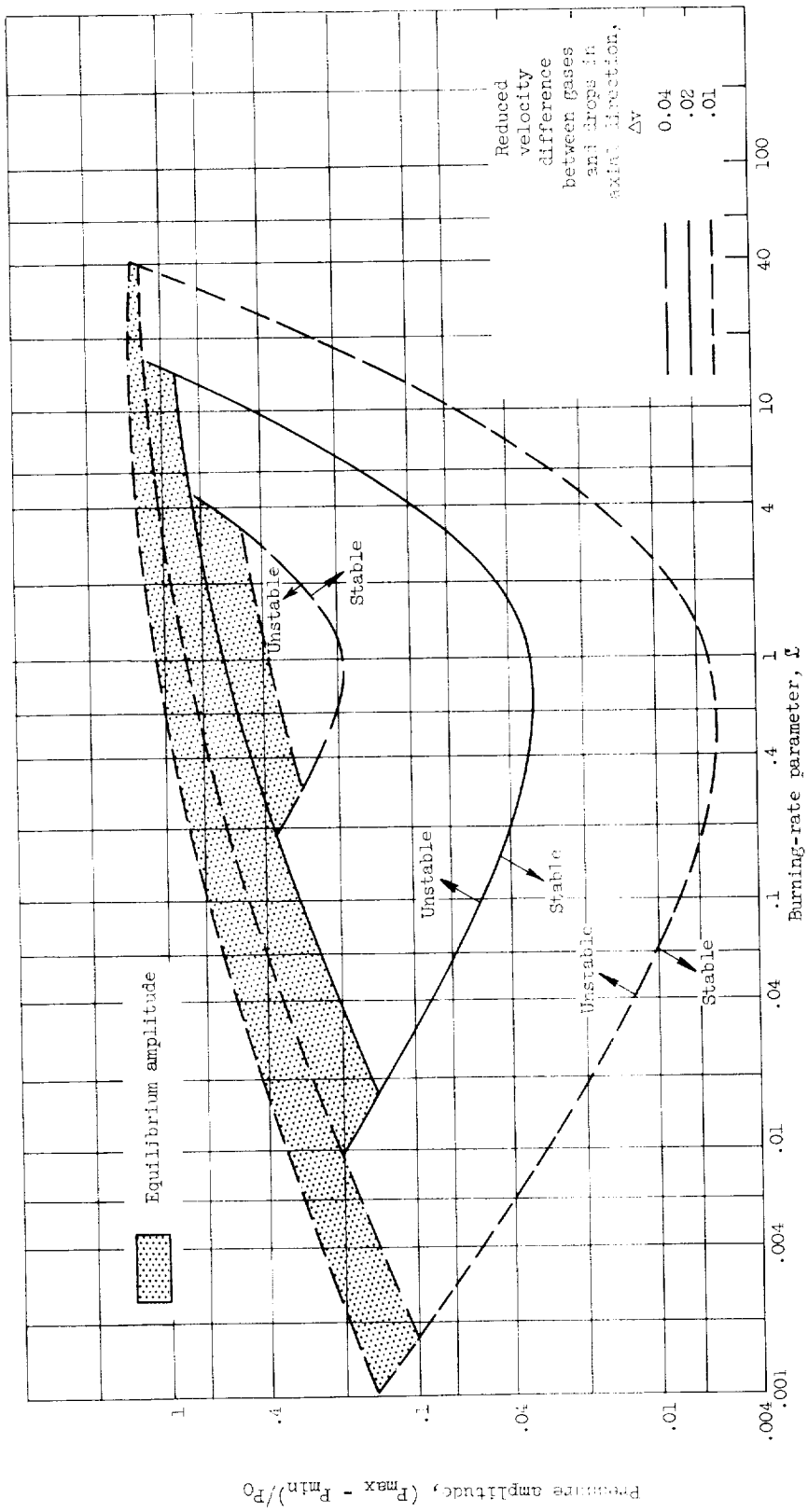

(a) Vaporization-rate model with various velocity differences.

Figure 8. - Stability limits of vaporization-rate and chemical-reaction-rate models.

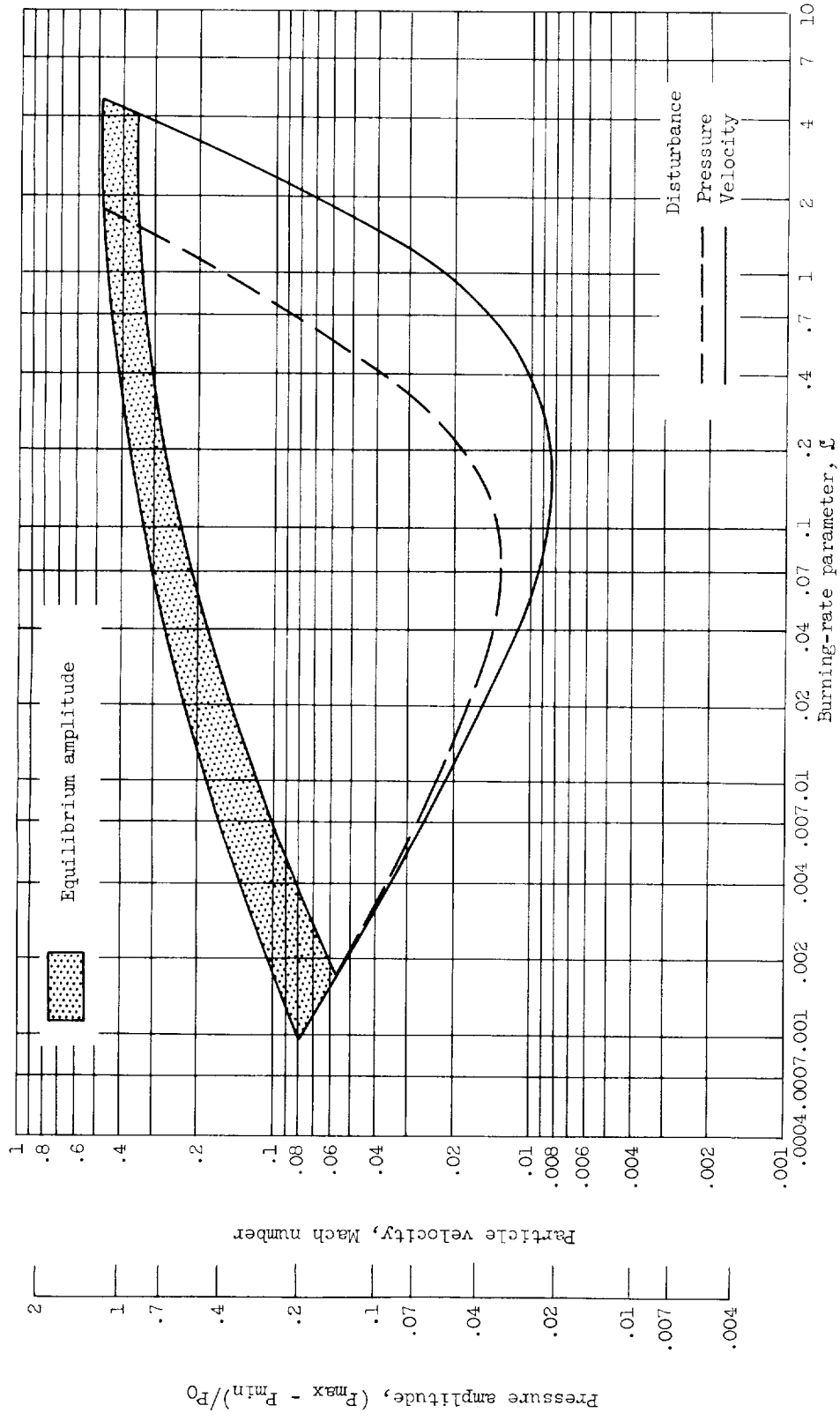

(b) Comparison of results obtained with initial pressure disturbance and those obtained with initial velocity disturbance; vaporization-rate model. Reduced velocity difference between gases and drops in axial direction, 0.02.

Figure 8. - Continued. Stability limits of vaporization-rate and chemical-reaction-rate models.

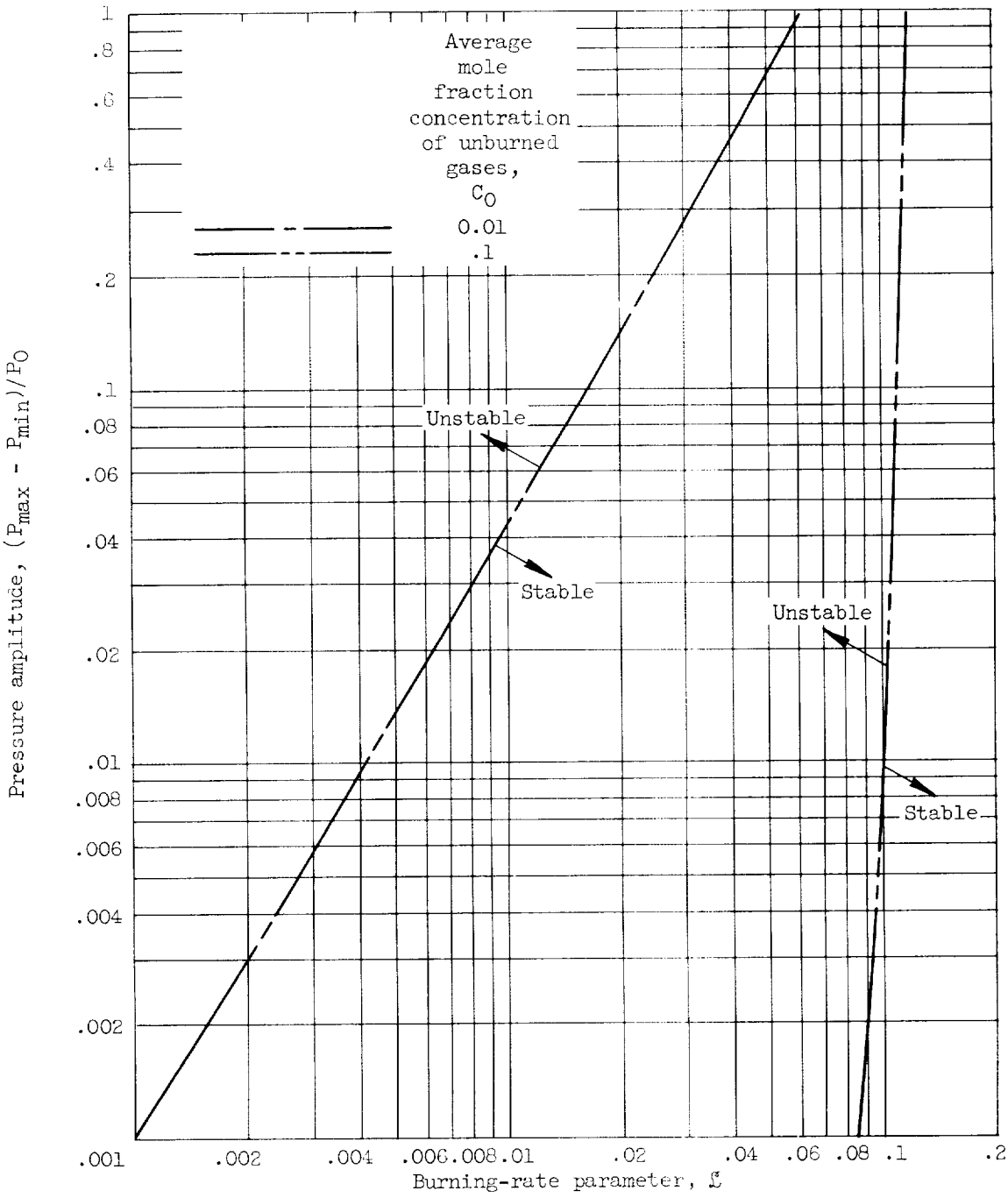

(c) Chemical-reaction-rate model.

Figure 8. - Continued. Stability limits of vaporization-rate and chemical-reaction-rate models.

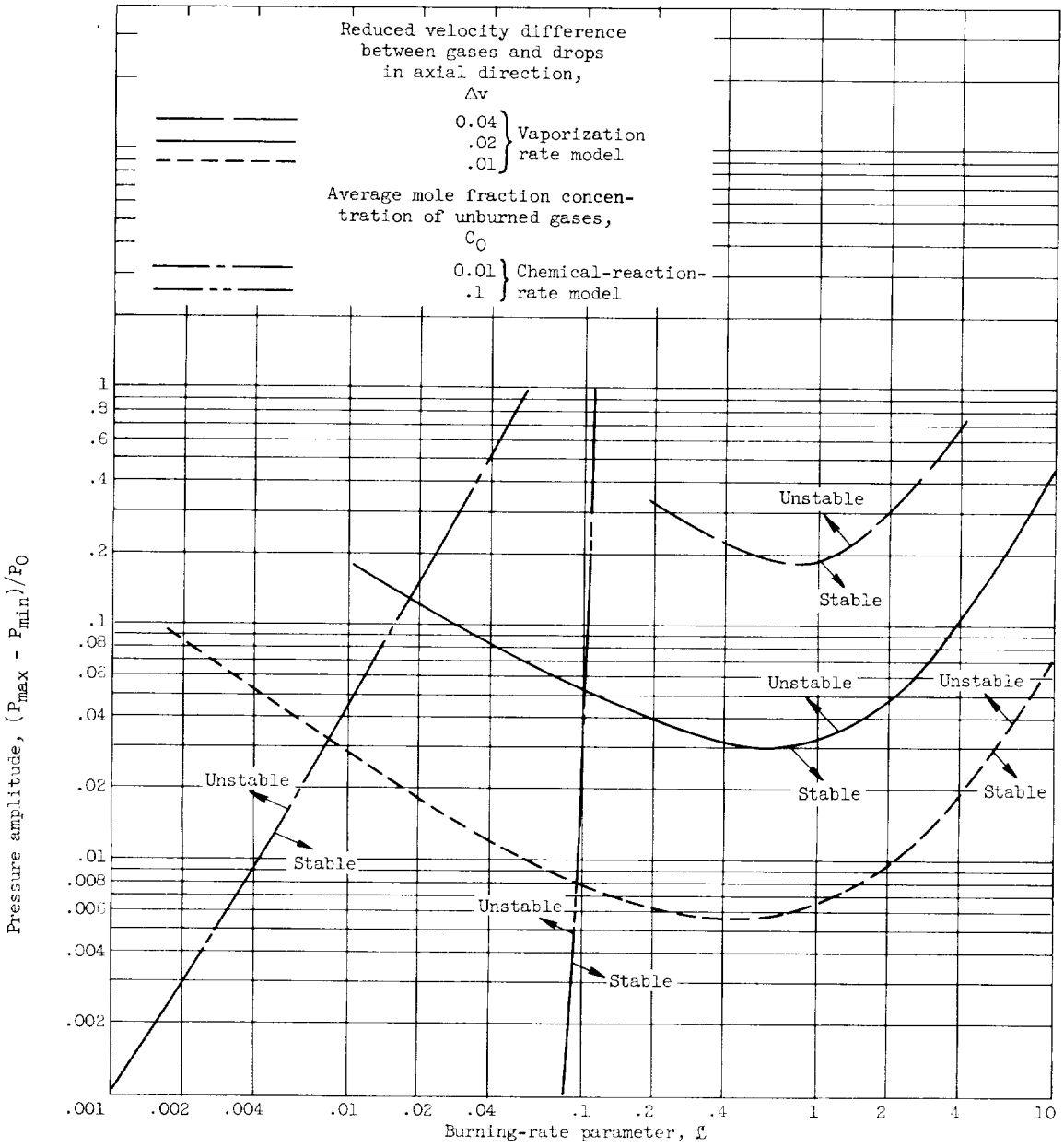

(d) Comparison of stability limits for both models.

Figure 8. - Concluded. Stability limits of vaporization-rate and chemical-reaction-rate models.